ASTRONOMY & ASTROPHYSICS
SUPPLEMENT SERIES

JANUARY II **1999**, PAGE 333

Astron. Astrophys. Suppl. Ser. **134**, 333–358 (1999)

The nature of arms in spiral galaxies

IV. Symmetries and asymmetries

M.S. del Río[1,2] **and J. Cepa**[2,3]

[1] Departamento de Astronomía, IFUG, Universidad de Guanajuato, 36000 Guanajuato, Mexico
[2] Instituto de Astrofísica de Canarias, E-38200 La Laguna, Tenerife, Spain
[3] Departamento de Astrofísica, Facultad de Física, Universidad de La Laguna, E-38071 La Laguna, Tenerife, Spain

Received April 24; accepted August 24, 1998

Abstract. A Fourier analysis of the intensity distribution in the planes of nine spiral galaxies is performed. In terms of the arm classification scheme of Elmegreen & Elmegreen (1987) seven of the galaxies have well-defined arms (classes 12 and 9) and two have intermediate-type arms (class 5). The galaxies studied are NGC 157, 753, 895, 4321, 6764, 6814, 6951, 7479 and 7723. For each object Johnson *B*-band images are available which are decomposed into angular components, for different angular periodicities. No a priori assumption is made concerning the form of the arms. The base function used in the analysis is a logarithmic spiral. The main result obtained with this method is that the dominant component (or mode) usually changes at corotation. In some cases, this change to a different mode persists only for a short range about corotation, but in other cases the change is permanent. The agreement between pitch angles found with this method and by fitting logarithmic spirals to mean arm positions (del Río & Cepa 1998b, hereafter Paper III) is good, except for those cases where bars are strong and dominant. Finally, a comparison is made with the "symmetrization" method introduced by Elmegreen, Elmegreen & Montenegro (1992, hereafter EEM), which also shows the different symmetric components.

Key words: galaxies: spiral — galaxies: structure of

1. Introduction

The majority of spiral galaxies, instead of showing two long and symmetric arms originating in the nucleus and extending all over the disc, present a more complex structure, sometimes with multiple arms, which can depart as satellites from a main arm. Johnson *B*-band images trace the distribution of young stellar population of spiral galaxies, and consequently, the arms, reasonably well. This is why we have chosen this band. Arms are fairly well described not only by logarithmic spiral but also by a number of other functions, such as Archimedean, Cotes, hyperbolic, gravitational and parabolic spirals (Danver 1942). The inherent problem in this kind of fit is that uncertainties set by arm distortions are too large to determine which is the best one (Kennicutt 1981). Another fundamental problem is the loss of bi-dimensional information, i.e. the radial and azimuthal intensity related to a particular fit. In order to solve these problems, Kalnajs (1975) introduced the Fourier transform method, later developed by Considère & Athanassoula (1982, 1988) and Puerari & Dottori (1992), to study the spiral structure of several galaxies. This method can be applied to H II region distributions or to broad-band images, and basically consists in choosing a set of functions and calculating the Fourier coefficients of the intensity (or H II number) distribution. The most used set of functions are logarithmic spirals, mainly because they are mathematically easy to handle and because they closely resemble real arm shapes, so that with few coefficients a very good description of the galaxy is reached. Other base functions could also be considered, with the requirements that they be *mathematically easy to handle*, fast to compute and reasonably similar in form to observed spirals. In summary, Fourier analysis of spiral patterns in galaxies provides quantitative data on arm multiplicity, form and radial extent, and does not assume that observed spiral structures are logarithmic. It merely analyses the observed distribution into a superposition of such logarithmic spirals.

Numerical orbit models (Patsis et al. 1991, and references therein; Patsis et al. 1994) seem to indicate that, because of the stochasticity of stellar orbits near corotation, spiral arms end at corotation or at the 4:1

Send offprint requests to: M.S. del Río
e-mail: sole@cibeles.astro.ugto.mx

inner Lindblad resonance (ILR), depending on the strength of the perturbation. These authors also claim that spiral structure extending beyond corotation as far as the outer Lindblad resonance (OLR) would be typical of barred spirals with their bars ending at corotation; otherwise a conspicuous gap in the spiral arms would appear. However, under conditions extracted from observations, N-body numerical simulations produce persistent spiral arms (Thomasson et al. 1990) which end at the OLR. According to the spiral density wave theory, although corotation is a singular region, short trailing waves can exist beyond corotation out to the OLR, while inside corotation, both short and long trailing and leading waves can exist (see, for example, Lin & Lau 1979, and references therein). On the other hand, several observational features can be readily understood if it is assumed that they mark the corotation region, thus implying that spiral arms end at the OLR, including spurs, gaps and interarm star formation (Elmegreen et al. 1989), breaks, bifurcations, changes of pitch angle, lower star formation in the arms compared with interarm star formation (Cepa & Beckman 1990a,b) and changes of arm skewness (Paper III). These features are usually present one at a time, and the gaps predicted by Patsis et al. (1991) are not generally present. Anyway, numerical simulations, analytical solutions and observational evidence coincide in that corotation is a singular region where the behaviour of density waves is not easy to predict. In this paper (the last of a series of four) we use Fourier transforms to complete the analysis of the sample of S(b-c) and SB(b-c) galaxies described in del Río & Cepa (1998a, hereafter Paper II), to analyse arm behaviour in the neighbourhood of the resonances and corotation determined in Paper III, together with the relative importance of the different arm components in these zones. Also, we compare the results with those obtained using the method of EEM.

In Sect. 2 we give a brief description of the data and the mathematical methods. Section 3 presents the analysis of spiral structure. Section 4 concerns to detailed analysis of each galaxy, and finally Sect. 5 shows the conclusions.

2. Data and methods

We use Johnson B-band CCD images of a group of spiral galaxies obtained at the prime focus of the 2.5 m Isaac Newton Telescope, at the Observatorio del Roque de los Muchachos, La Palma. The images were reduced using standard routines, with a seeing-limited angular resolution close to 1 arcsec. The observations and data reduction are described in detail in Paper II. In their original form (before deprojection) the orientation is north–right, east-top. In this paper all images are deprojected. The positive $\widehat{x}$-axes corresponds to the PAs listed in Table 2.

2.1. Fourier transform method

A complete and detailed description of this method can be found in Puerari & Dottori (1992). We give a brief review here of the procedure, and of the notation and formulae used.

We consider the decomposition of a given distribution of intensities of a set of continuous two-dimensional coplanar points into a superposition of m-armed logarithmic spirals. Each point, associated with a pixel of the image, with polar coordinates (r_j, θ_j) in the galaxian plane, is weighted by the intensity of the corresponding pixel. An m-armed logarithmic spiral is expressed by $r = r_0 \exp(-(m/p)\theta)$, where m is the number of arms, i.e. the angular periodicity number, and p is related to the pitch angle i of the spiral via the relation $\tan i = -m/p$[1]. The distribution of the points that follow the former conditions can be written in terms of δ-functions, and its Fourier transform is then expressed by

$$A(m,p) = \int_{-\infty}^{+\infty} \int_{-\pi}^{+\pi} \sum_{i=1}^{I} \sum_{j=1}^{J} \omega_{ij} \delta(u - u_{ij}) \delta(\theta - \theta_{ij}) \times \exp\left[-i(pu + m\theta)\right] \mathrm{d}u\mathrm{d}\theta / \sum_{i=1}^{I} \sum_{j=1}^{J} \omega_{ij}, \quad (1)$$

where ω_{ij} is the weight of the point (ij), r_{ij} and θ_{ij} its deprojected radial and angular coordinates and $u_{ij} \equiv \ln r_{ij}$. Eq. (1) has the simpler form:

$$A(m,p) = \left(\sum_{i=1}^{I} \sum_{j=1}^{J} \omega_{ij} \exp\left[-i(pu + m\theta)\right] \right) / \sum_{i=1}^{I} \sum_{j=1}^{J} \omega_{ij}. \quad (2)$$

The complex surface brightness of each m component is the sum of the inverse Fourier transforms of the complex function $|A(m,p)|$:

$$S(u,\theta) = \frac{1}{e^{2u}} \cdot \frac{\sum_{i=1}^{I} \sum_{j=1}^{J} \omega_{ij}}{4\pi^2} \times \sum_{m} \int_{-\infty}^{+\infty} G_m(p) A(m,p) e^{i(pu + m\theta)} \mathrm{d}p. \quad (3)$$

$G_m(p)$ is a high frequency filter used to emphasize the main component, i.e. the spiral with $\tan i = -m/p^m_{\max}$:

$$G_m(p) = \exp\left(-\frac{1}{2} ((p - p^m_{\max})/25)^2 \right) \quad (4)$$

where $p^m_{\max}$ is the value of p^m for which the amplitude of $|A(m,p)|$ is a maximum. This filter is also used to smooth the Fourier coefficient spectra at the ends of the interval, so $|A(m,p)|$ goes to zero for large values of $|p|$.

The righthand side of Eq. (3) can be separated by variables in the form:

$$S(r,\theta) \equiv S(u,\theta) = \sum_{m} S_m(u) \cdot e^{im\theta}, \quad (5)$$

[1] The $|A(m,p)|$ coefficients represent the contribution to the m-symmetry of a spiral whose pitch angle is $i = \mathrm{arctg}(-m/p)$.

where

$$S_m(u) = \frac{1}{e^{2u}} \frac{\sum_{i=1}^{I} \sum_{j=1}^{J} \omega_{ij}}{4\pi} \int_{-\infty}^{\infty} G_m(p) A(m,p) e^{ipu} \mathrm{d}p. \quad (6)$$

Finally, to construct the different m-images, denoted as S_m ($S_m(r)$ and S_m do not vary so much when are calculated without $G(p)$ filter, only the arm edges are slightly noisier), we take the real part of the $S_m(r)e^{i\theta m}$, giving all negative pixels value zero.

The relative importance of the different spiral modes can be estimated from

$$f_m = \frac{S_m}{S_1 + S_2 + S_3 + S_4 + S_5}, \quad (7)$$

with

$$S_m = \int_{r_1}^{r_2} S_m(r)\, \mathrm{d}r,$$

where we have changed S_6 to S_1 from the original formula of Considère & Athanassoula (1988), because in our decomposition the latter is simply noise, whereas the former keeps information, and the lower limit in the integration from 0 to r_1, because our values usually diverge at $r \sim 0$, and we wish to avoid the influence of oval bulges, which favour S_2 components.

2.2. Symmetric and asymmetric images

This method has been developed and applied by EEM and consists in decomposing a given image into images of different degrees of symmetry through rotations and subtractions, thereby obtaining the bi-, tri- and four-symmetric images S2, S3 and S4, respectively, together with the asymmetric image A2. This method maintains the non-linear spiral arm form, without introducing spurious inter-arm components. The authors also claim that this technique shows the $m = 1, 2, 3, 4, ...$ sub-components simultaneously over the whole image, which prevents confusion with field stars or star formation zones.

According to EEM, not only do galaxies apparently showing a high degree of symmetry, such as NGC 157 and NGC 4321 in this sample, have an important tri-symmetric component that is not evident in the images, but even galaxies with lower symmetry, such as NGC 6764 and NGC 7723, also possess this tri-symmetry. The 3-S structure extends from the 3:1 ILR to the 3:1 OLR, and, correspondingly, the 4-S structure from the 4:1 ILR to the 4:1 OLR.

3. Analysis of spiral structure

With the method of Fourier decomposition of spiral structure, an ideal logarithmic spiral presents a single-peaked spectrum of intensity normalized to unity, centred on a value of $p^m_{\max}$ related with a pitch angle $p^m_{\max} = -m/\tan i$. Real galaxian arms are approximations to logarithmic spirals, so that the corresponding peak is of lower amplitude, larger, and/or asymmetric. Also, if the deprojection is not correct, a spurious peak at $p = 0$ can appear, with an intensity that increases with inclination angle, because the resulting distribution tends to a straight line as the inclination increases, and the Fourier transform of radial arms represent $i \sim 90°$, i.e. $p^m_{\max} \sim 0$. When the bar is strong and arms are not symmetric and/or very weak, a component also appears at $p^2_{\max} = 0$, even if deprojection is correct. Nevertheless, in cases where one arm is brighter than the other, the $m = 1$ component gives a much more reliable pitch angle in better agreement with those calculated by other methods.

Through the $S_m(r)$ functions of a given flux distribution, we can determine the angular periodicity which better represents the flux distribution at each radius, i.e. the predominant m for each galactocentric distance indicates that at this radius the intensity distribution shows a preferential angular separation of $2\pi/m$. Although it is tempting to associate the minima of the $|S_m(r)|$ functions with resonances, it is necessary to add a word of caution, because there are several other ways in which such minima can occur. In fact, near corotation, we can expect not only a lower flux but also a gap, a change in pitch angle, skewness or a difference of sign in mean position in different bands (Paper III). We show in this paper that not only a local minimum occurs near corotation, but also that the dominant mode changes.

To apply the Fourier transform method, we have kept in the calculations only those pixels which are brighter than a given luminosity threshold and within a given deprojected distance from the galaxian center. Both these limits were determined with the help of isophotal contour maps, and the brightness threshold was taken so as to include not only the bright spiral arms but also the inter-arm and outer-disc regions. In fact, both conditions are equivalent because, once the image is deprojected, outer isophotes are roughly circular. So we must reach a compromise regarding most of the flux be included and do not take noise levels into account, or even the axisymmetric disc contribution. With all this in mind, we see that the chosen contours vary between $\sim 2.7\,\mathrm{mag}/''^2$ lower than limiting magnitude in NGC 157 (i.e. the equivalent contour to $23.11\,\mathrm{mag}/''^2$) and $\sim 0.07\,\mathrm{mag}/''^2$ lower than limiting magnitude in the faintest galaxy, NGC 6764 (the contour equivalent to $24.94\,\mathrm{mag}/''^2$).

Also, to compare with the method developed by EEM, we have eliminated field stars because they introduce a lot of noise. Since they are usually randomly distributed over each frame and appear in all coefficients, and because of the finite width of these coefficients, when we reconstruct the S_m images, stars appear as small arcs, not as point-like structures. This phenomenon is not present in the EEM method, because all asymmetric features, such as stars, remain in the A2 image.

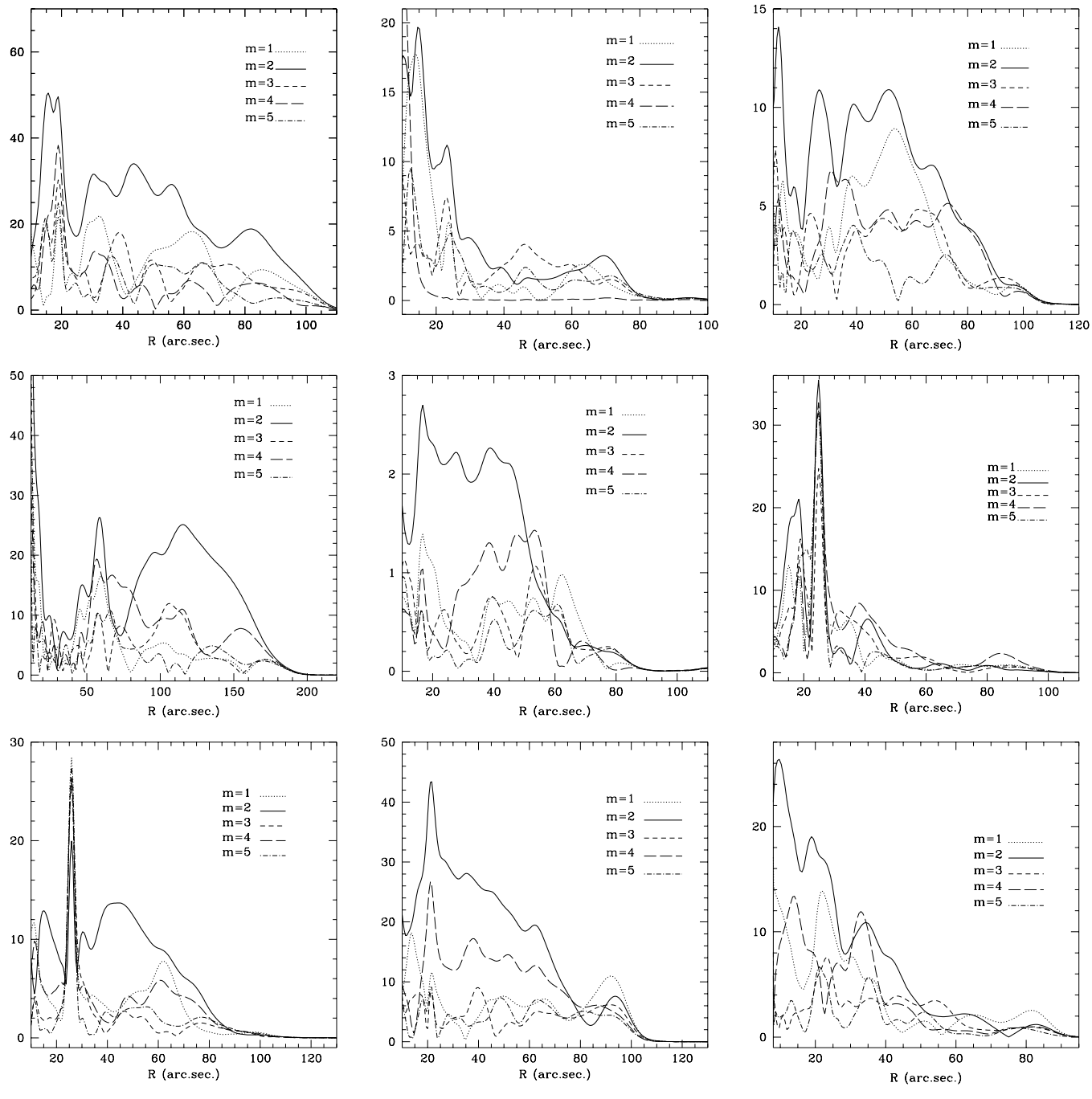

Fig. 1. $S_m(r)$ functions. From left to right and from top to bottom: NGC 157, NGC 753, NGC 895, NGC 4321, NGC 6764, NGC 6814, NGC 6951, NGC 7479 and NGC 7723

In order to reduce the noise level in the coefficients as much as possible, we remove the stars by using a simple technique. The flux around stars is calculated, and then the stars are substituted by this mean value (except when they are very close to the arms, in which case we prefer to leave them in the image). The results with and without field stars are shown in Fig. 3.

Although we are mainly interested in decomposing images in different angular modes, it is also possible, with the Fourier transform method, to estimate the inclination (ω) and position angles (PA). This procedure assumes that the arms can be reasonably approximated by logarithmic spirals, so that their Fourier spectrum has a single peak centred around $p_{\max}$. To calculate the best pair of values of PA and ω, we can follow Considère & Athanassoula (1988)

method of maximizing the value of the dominant component (usually $m = 2$) while minimizing the component around $p^2 = 0$, or we can follow Puerari & Dottori (1992), who maximize the signal-to-noise ratio of the dominant coefficient.

For each galaxy in our sample we first consider a wide range of angles, for for both PA and ω (an interval of 67° centred on the values found in Paper II, assuming that the outermost deprojected isophotes are circular in Considère & Athanassoula 's method and 13° for Puerari & Dottori's method, with a spacing grid of ΔPA and $\Delta\omega = 3°$. Calculation of the spectra for these deprojection parameters allowed us to find a maximum, according to the criteria mentioned above. Centred on the new pair of values (PA, ω) which maximizes the previous ratios, we recalculated the Fourier coefficients using a finer grid, with steps of one degree, over a range of 7° about these values. The results and comparisons with previous work are summarized in Table 2. Nevertheless, these methods present serious problems, which we will discuss later (Figs. 6, 7, 8 and 9).

4. Results

In the following subsections we show, for each galaxy of the sample, the $|A(p, m)|$ spectra, with and without noise from field stars, and the $|S_m(r)|$ functions for all the galaxies in our sample. The spectra for $1 \leq m \leq 6$ are shown in Fig. 3 and the $|S_m(r)|$ functions for $1 \leq m \leq 5$ in Fig. 1. In all the galaxies in our sample the dominant component is $m = 2$, except in the case of NGC 6814, which shows a dominant four-armed pattern.

4.1. NGC 157

The first impression of this galaxy is that its entire surface is covered with luminous spiral arm segments, intermingled with dust lanes. The most prominent dust lane is on the concave side of the arm that extends from the bulge (very small and without structure) to the north. This lane crosses the arm at $40'' \lesssim R \lesssim 45''$ only once. Burbidge et al. (1961) found a very flat, almost linear, relative density curve i.e. there is not much mass concentration in the central region of this galaxy. It has been identified as a starburst galaxy (Devereux 1989), with strong H_α and [N II] lines. Zasov & Kyazumov (1981) found very symmetric arms, which suggests there is no substantial large-scale non-circular motion in the spiral zone; but at $R > 55''$ on the northern side, there is an abrupt fall-off in rotational velocity, which Burbidge et al. (1961) did not find in their rotation curve, calculated from H_α and [N II] λ6583 emission lines. This effect cannot be due to a companion, because the nearest galaxy, NGC 255, is somewhat more than three degrees away ($\sim$1.16 Mpc).

Table 1. Relative weight (in %) of the different symmetric components obtained by Fourier transforms and Eq. (7). It is noticeable that in three galaxies the percentage changes after corotation (in NGC 753, NGC 6814 and NGC 7479), in other three galaxies, after or before corotation, two modes have similar weights (NGC 895, NGC 4321 and NGC 6764), and the final three maintain the same and lonely dominant component

		Before CR	After CR	Total
NGC 157	$m = 1$	0.214	0.223	0.219
	$m = 2$	0.335	0.408	0.364
	$m = 3$	0.157	0.146	0.152
	$m = 4$	0.169	0.074	0.131
	$m = 5$	0.122	0.148	0.133
NGC 753	$m = 1$	0.248	0.118	0.222
	$m = 2$	0.373	0.271	0.352
	$m = 3$	0.126	0.420	0.185
	$m = 4$	0.118	0.006	0.096
	$m = 5$	0.139	0.182	0.143
NGC 895	$m = 1$	0.216	0.110	0.206
	$m = 2$	0.362	0.336	0.360
	$m = 3$	0.153	0.115	0.149
	$m = 4$	0.175	0.323	0.189
	$m = 5$	0.093	0.114	0.094
NGC 4321	$m = 1$	0.189	0.082	0.132
	$m = 2$	0.289	0.491	0.398
	$m = 3$	0.134	0.163	0.150
	$m = 4$	0.251	0.193	0.219
	$m = 5$	0.134	0.069	0.099
NGC 6764	$m = 1$	0.144	0.212	0.169
	$m = 2$	0.500	0.244	0.407
	$m = 3$	0.104	0.175	0.131
	$m = 4$	0.195	0.227	0.205
	$m = 5$	0.055	0.139	0.085
NGC 6814	$m = 1$	0.199	0.167	0.188
	$m = 2$	0.263	0.178	0.231
	$m = 3$	0.169	0.227	0.192
	$m = 4$	0.171	0.317	0.224
	$m = 5$	0.196	0.109	0.163
NGC 6951	$m = 1$	0.213	0.103	0.197
	$m = 2$	0.447	0.353	0.434
	$m = 3$	0.073	0.123	0.080
	$m = 4$	0.183	0.248	0.192
	$m = 5$	0.082	0.170	0.095
NGC 7479	$m = 1$	0.125	0.309	0.146
	$m = 2$	0.433	0.195	0.407
	$m = 3$	0.092	0.189	0.103
	$m = 4$	0.250	0.169	0.241
	$m = 5$	0.097	0.136	0.101
NGC 7723	$m = 1$	0.218	0.160	0.200
	$m = 2$	0.394	0.329	0.374
	$m = 3$	0.091	0.212	0.129
	$m = 4$	0.222	0.175	0.206
	$m = 5$	0.073	0.122	0.088

Another important feature of the rotation curve is the long, almost linear, branch, that extend about 8 or 9 kpc from the nucleus. Within the errors it remains constant over this interval. Although other galaxies have this kind

of behaviour (like NGC 7479 in our sample), it is not a frequently occurring case. This feature of the rotation curve is incompatible with an exponential decrease in galaxian mass surface (see Zasov & Kyazumov 1981).

With the azimuthal method (Paper III) we found a change in the sign of the difference in the B- and I-band mean position, as well as in the sign of the profile skewness in the B band at $R \sim 40''$. Also, a dust lane crosses the northern arm at approximately this distance. All this evidence leads us to the conclusion that CR is found at $R \sim 40''$. In addition, and in spite of the fact that due to the high bi-symmetry of this galaxy the $m = 2$ component is dominant at all radii, we found a local minimum at $S_2(r)$ near $R \sim 40''$, coinciding with an increase in the other (secondary and odd) components, $S_3(r)$ and $S_5(r)$.

This highly symmetric galaxy shows a spectrum with a two-armed component dominating to the outer part of the disc (Figs. 2 and 4). There is a small radial range $70'' \lesssim R \lesssim 75''$, where secondary components, as $m = 1$ and $m = 5$ dominate slightly over $m = 2$ (Fig. 1), but the OLR is located at this radius (Paper III). In the same figure, near corotation, $R \sim 40''$, we find a local minimum at $S_2(r)$ and local maxima of the other modes. The Fourier coefficients show a narrow peak at $m = 2$ centred on $p^2_{\max} = 3$, which corresponds to a two-armed spiral with pitch angle $i \sim 34°$, slightly higher than found the from azimuthal profiles (Paper III). If we fit a Gaussian to the main peak, the maximum is shifted to $p^{\rm g}_{\max} = 4.5$ which leads to a pitch angle ($i^{\rm g} \sim 24°$) much more similar to the previous one. The use of Gaussians is justified because the p values are integers, so the only pitch angles possible are 90°, 63°, 45°, etc., while, as we mentioned before, $|A(m,p)|$ represents the "weight" that a spiral with pitch angle i has in the m-order symmetry. In this case, with the Gaussian fit we found a reasonable average of such values. A secondary maximum at $m = 1$, does not correspond to a one-armed spiral pattern, but reflects the star formation burst with a strong asymmetric component (Figs. 2 and 4).

Using the EEM method, an elongated bulge can be seen from which emerges a small "bar" of $40''$, from which, in turn, two vigorous arms originate. But this "bar" is probably just an artifact of the symmetrizing method, just like the dust lane in the southern arm, which is not present in the original image. Dust is present in the S2 image on the concave side of the arms, until $R \sim 40''$, beyond which the dust lanes cross to the convex side much more inconspicuously. Finally, the arms end at $R \sim 70''$, where the OLR could be located (Paper III). The ratio between the radius of both resonances, OLR/CR ~ 1.75 is in perfect agreement with that found by EEM. Higher-symmetry images, as in the method of Fourier decomposition, do not show very important structure, despite that found by EEM.

4.2. NGC 753

In the image of this apparently small galaxy we can distinguish a brilliant and elongated nucleus. From this nucleus emerge two main arms, with very patchy star formation, and of very irregular brightness, becoming almost invisible beyond 180° from their were origin. Around these two arms several others are wound; they are more extended but much weaker and give the impression of a light pinwheel expanding from the nuclear zone to the outest parts of the optical disc. This open structure may be due to a relative close companion, NGC 759, at 0.44 Mpc and $\Delta v \sim 22\,\mathrm{km\,s^{-1}}$ (with $H_0 = 75\,\mathrm{km\,s^{-1}\,Mpc^{-1}}$).

The skewness and mean position difference in this galaxy were really difficult to measure (Paper III) and none of the results was conclusive, all instead indicating a special situation around $R \sim 30''$. The pitch angle found by exponential fitting to mean positions in the arms has an abrupt change (from 13° to 24°) at this position; the skewness and mean position difference behave in a distinct manner before and after this point. Finally, the Fourier transform analysis supports the idea that CR is located at $R \sim 30''$; at this distance ($\sim 28''$) we found a local minimum at $S_2(r)$, which is the endpoint of the stronger and more symmetric arms, and close to this radius ($R \sim 38''$) $S_3(r)$ becomes the main component until the end of the visible disc.

Fourier decomposition is not expected to provide much clarification; in fact, the spectra of this galaxy show a noisy two-armed component (with $S/N \sim 17$), and a moderately strong three-armed component, while the rest of components are not at all significant. The maximum in the $S_2(r)$ mode is located at $p^2_{\max} = -5$, which leads to a pitch angle $\approx 22°$, somewhat less than that found with a logarithmic fit ($\sim 28°$). We must take into account that the signal is quite noisy. If we estimate the maximum position with a Gaussian fit, we find $p^{\rm g}_{\max} = -3.88$, or a pitch angle $\approx 27°$, in much better agreement with the logarithmic fit. In both cases, this relatively good agreement with a poor fit is due to the mixing of the inner (more closed) and outer (much more open) arm shapes. The Fourier transform also treats the arm as there were no breaking; in fact the first pitch angle (which is provided by a maximum in the $m = 2$ spectrum) is closer to the value calculated only for the inner arm (where the image $m = 2$ is more intense) using a logarithmic fit, than to the value obtained from the outer arm.

The bi-dimensional distribution of $S_m(r)$ confirms that found from the spectra. In spite of the low intensity of all components, the bi-dimensional distribution S_2 stands out from the others, showing two short tightly wound arms around the nucleus that split at $R \sim 30''$, one part following the same path part, and the other opening out, as shown in the logarithmic fit (Paper III) and S2 image. In the second place, $m = 1$ reveals irregular star formation in zones close to the nucleus, with a shape very similar

Table 2. Data marked with † are from de Vaucouleurs, those marked with ‡ are from Grosbøl. For NGC 4321 whe have used $i = 31°$ and PA $= 151°$, from Cepa et al. Data marked with * have been calculated in del Río & Cepa (1998b). Finally, those marked with ** and § have been calculated in this work, the former correspond to Considère & Athanassoula method, and the last to Puerari & Dottori method. Angles for NGC 6814 marked with * have been calculated with $m = 4$ as dominant mode

Object	PA†	$\omega^\dagger$	PA‡	$\omega^\ddagger$	PA*	ω^*	PA**	ω^{**}	PA§	$\omega^\S$
NGC 0157	40°	50°	35°	45°	45°	50°	26°	47°	45°	55°
NGC 0753	125°	39°	112°	46°	126°	45°	119°	43°	132°	53°
NGC 0895	65°	45°	116°	50°	114°	50°	126°	54°	111°	56°
NGC 4321	30°	32°	58°	25°	151°	31°	115°	43°	157°	36°
NGC 6764	62°	56°	62°	62°	59°	59°	64°	67°	63°	58°
NGC 6814		21°	167°	7°	167°	7°	150°	0°	158°	−1°
NGC 6814*							135°	41°	161°	15°
NGC 6951	170°	34°	157°	44°	157°	44°	118°	39°	154°	52°
NGC 7479	25°	40°	39°	45°	39°	45°	21°	59°	45°	40°
NGC 7723	35°	47°	38°	47°	37°	48°	46°	46°	30°	57°

to that of A2. The wide fringe around $R \approx 50''$ is consequence of increasing intensity at the end of the eastern arm. The first relative minimum in $S_2(r)$ should be produced by internal dust located symmetrically with respect to the centre and perpendicular to the major axis, because all components are affected. The next minimum, at $R \sim 28''$, matches reasonably well with the sign change in $S^{\rm B}$ and $\overline{\theta^{\rm B}} - \overline{\theta^{\rm I}}$ and with a sharp change in pitch angle (see Paper III). This is another indication that supports the idea that CR is near $R \sim 30''$. The next relative minimum, at $R \sim 38''$, marks the end of the more intense arms, and a change in dominant mode from the $m = 2$ dominant pattern (due to the strong arms) to $m = 3$, until $R \sim 60''$ (due to the eastern arm and the external splitting of the western arm). However, the emission in this zone is too weak for these features in the S3 image to be appreciated.

4.3. NGC 895

This galaxy has two long and symmetric arms, as can be see in Figs. 2 and 4, and, external to these, several others that are fainter and rather patchy, as would correspond to a prototypical class 9 galaxy. The $m = 2$ component shows a high, narrow peak, with $S/N \sim 61$, clearly dominating over the other components. The high values of the $m = 4$ and $m = 6$ components, in addition to harmonics of $m = 2$, probably reflect the structure of these secondary arms. However, the $m = 1$ component represents the asymmetric star formation produced in the western arm, which is wider than the eastern one. The maximum of $|A(2, p)|$ is $p^2_{\rm max} = -4$ (-3.55 after a Gaussian fit), which leads to a pitch angle of $26°(29°)$, in very good agreement with the value found using a simple least-squares fit of a logarithmic function to the mean positions, in only one arm (Paper III). This is obviously due to the high degree of symmetry in both arms. Decomposing the image following the EEM method reveals that 79% of the total emission comes from S2, and that S3 and S4 have only remains of axisymmetric and bi-symmetric images, respectively. The arms are relatively short and end in the most intense star formation just beyond corotation, although the weakest parts reach the OLR. At $R \sim 75''$, where corotation is located (Paper III), the m-components show a small change in the dominant mode over $\sim 10''$, where the main component, $S_2(r)$, drops to a local minimum, while $S_4(r)$ exceeds slightly this value.

The logarithmic fit of mean positions (Paper III) is exceptionally good in this highly bi-symmetric galaxy, whose arms seem to end slightly beyond CR. It might be that the high degree of bi-symmetry occurs because the arms almost coincide with the main part of the pattern. As previously mentioned, this is an observational confirmation that, before corotation, short and long waves are found, whereas, beyond corotation, only short trailing waves, which only just reach the OLR, are seen. In Fig. 1c it can be seen that the $S_2(r)$ component strongly dominates the others, and that at CR ($\sim 75''$) there is a soft local minimum of $S_2(r)$ as well as slight local maxima of $S_4(r)$ (which even overshadows $S_2(r)$, $S_5(r)$ and $S_6(r)$, which are not present in the figure). The bi-dimensional $S_m(r)$ distribution shows a galaxy with a complex structure, with two long arms that originate in the very inner part of the small bulge, an S_1 component that reproduce the different star formation rates of both main arms, and S_3 and S_4 components that reproduce the outer and fainter arms.

The first pronounced local minimum in $S_2(r)$ is at $R \sim 20''$, but inside this radius a small spiral is enclosed, which is not visible either in the flux image (Paper II) or in S2. A second important minimum occurs at $R \sim 32''$, close to the theoretical 3:1 ILR position. The last $S_2(r)$ minimum, at $R \sim 75''$, coincides with the end of the brightest arms, with the sign change in $\overline{\theta^{\rm B}} - \overline{\theta^{\rm I}}$, with the tendency change in B skewness (Paper III) and with a change in dominant mode, which passes from $S_2(r)$ to $S_4(r)$ over a small interval of $10''$.

Again we have found serious anomalies near corotation.

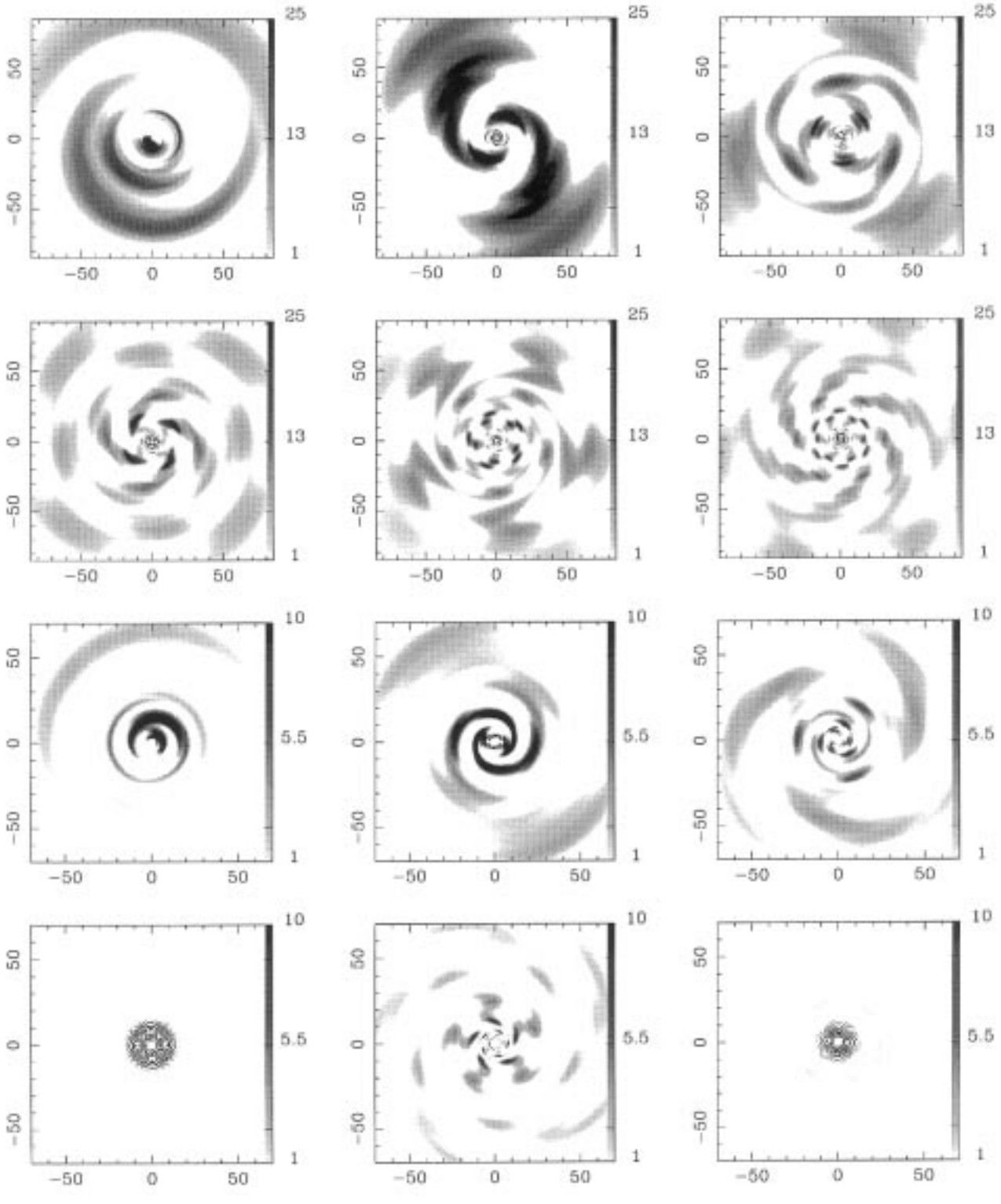

Fig. 2. Fourier anti-transforms. Top: NGC 157. Bottom: NGC 753

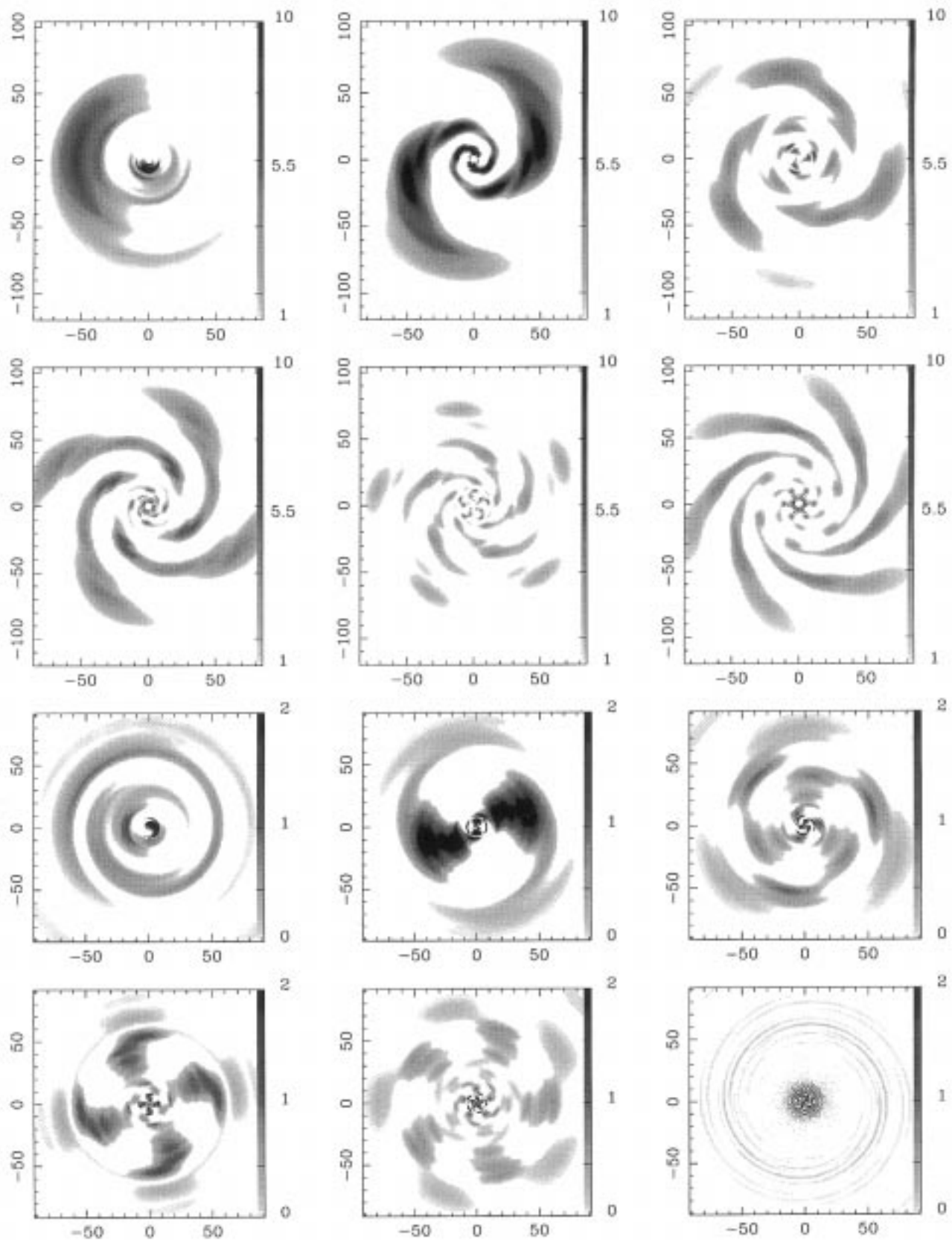

Fig. 2. (continued) Fourier anti-transforms. Top: NGC 895. Bottom: NGC 6764

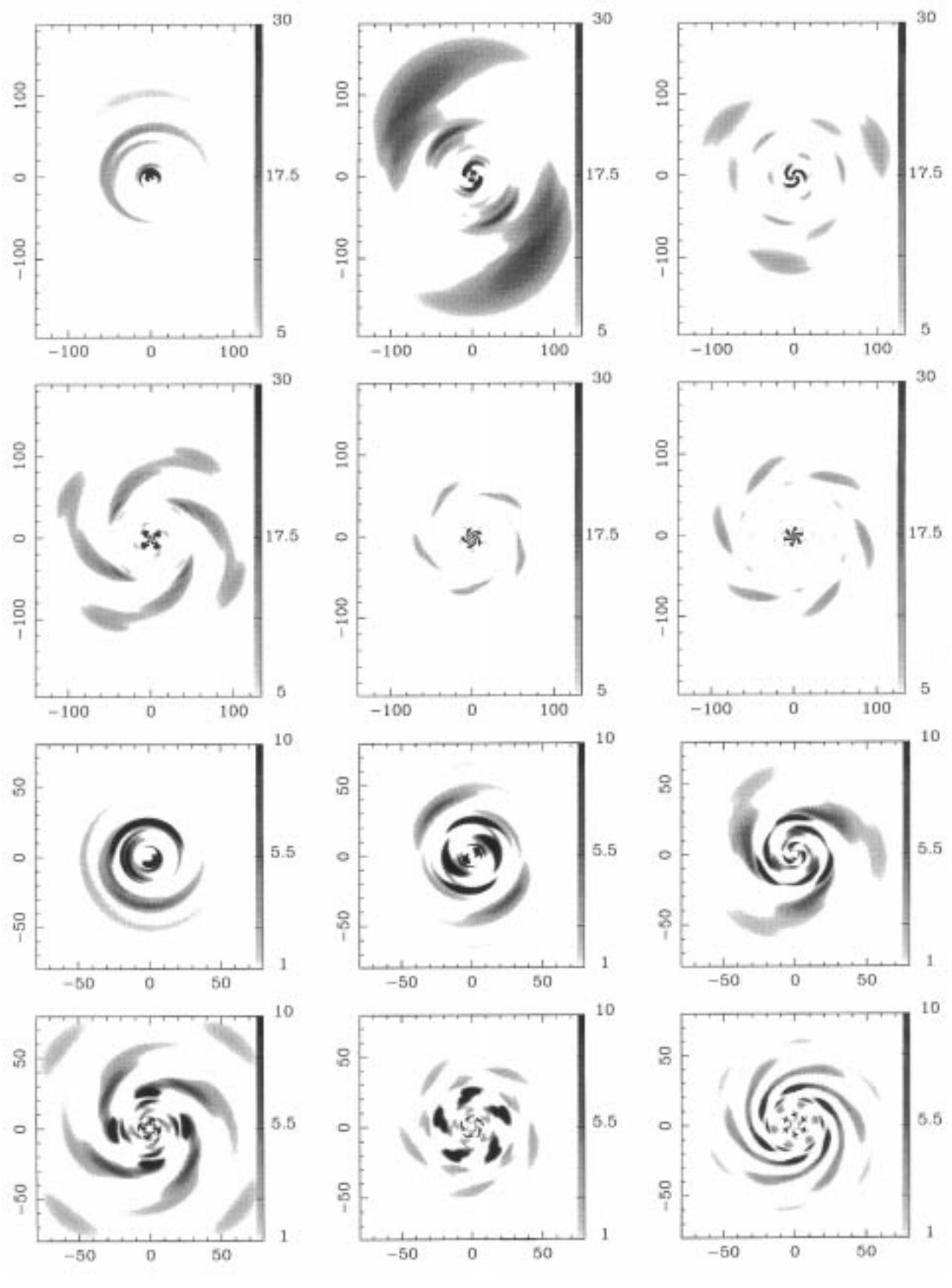

Fig. 2. (continued) Fourier anti-transforms. Top: NGC 4321. Bottom: NGC 6814

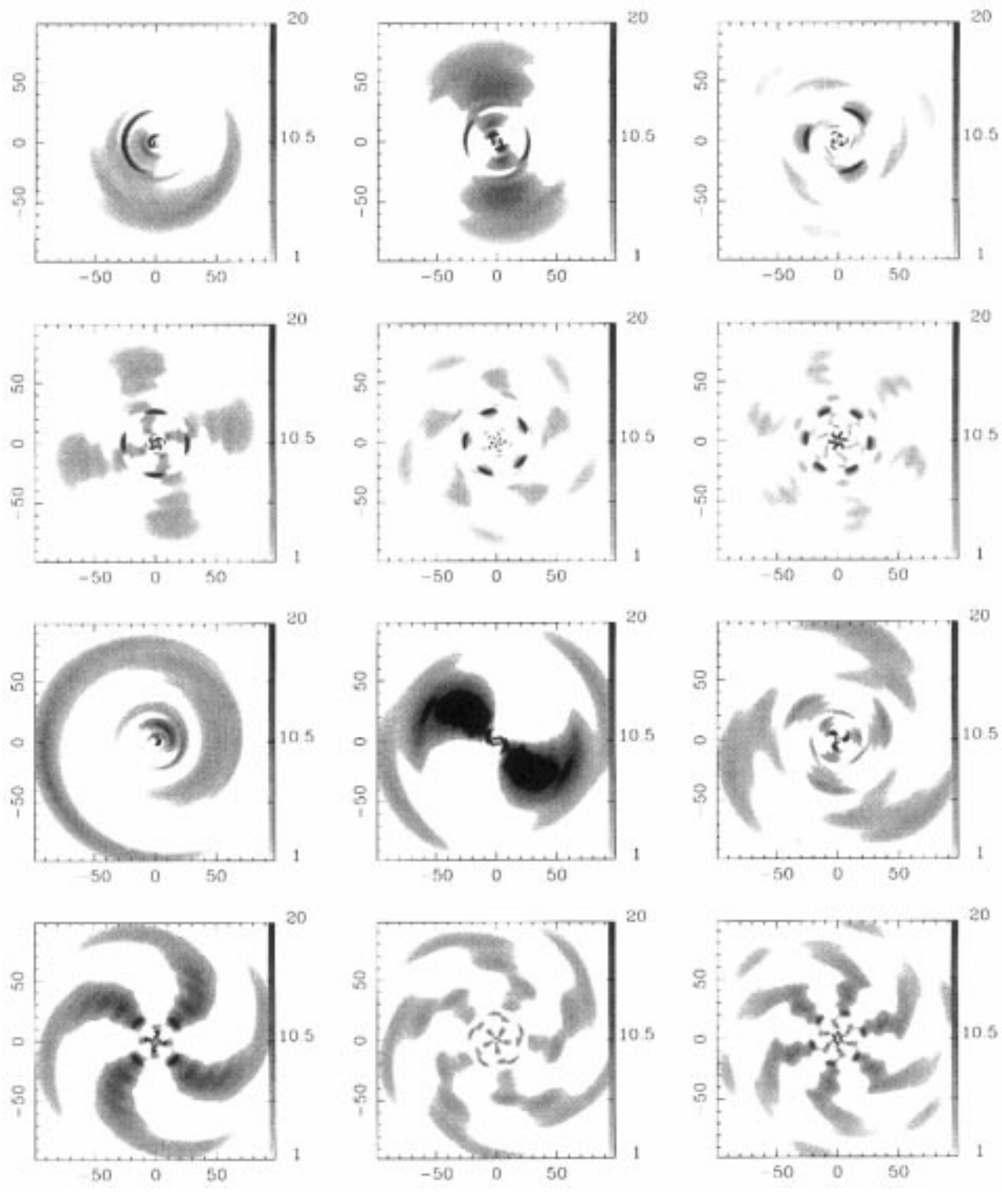

Fig. 2. (continued) Fourier anti-transforms. Top: NGC 6951. Bottom: NGC 7479

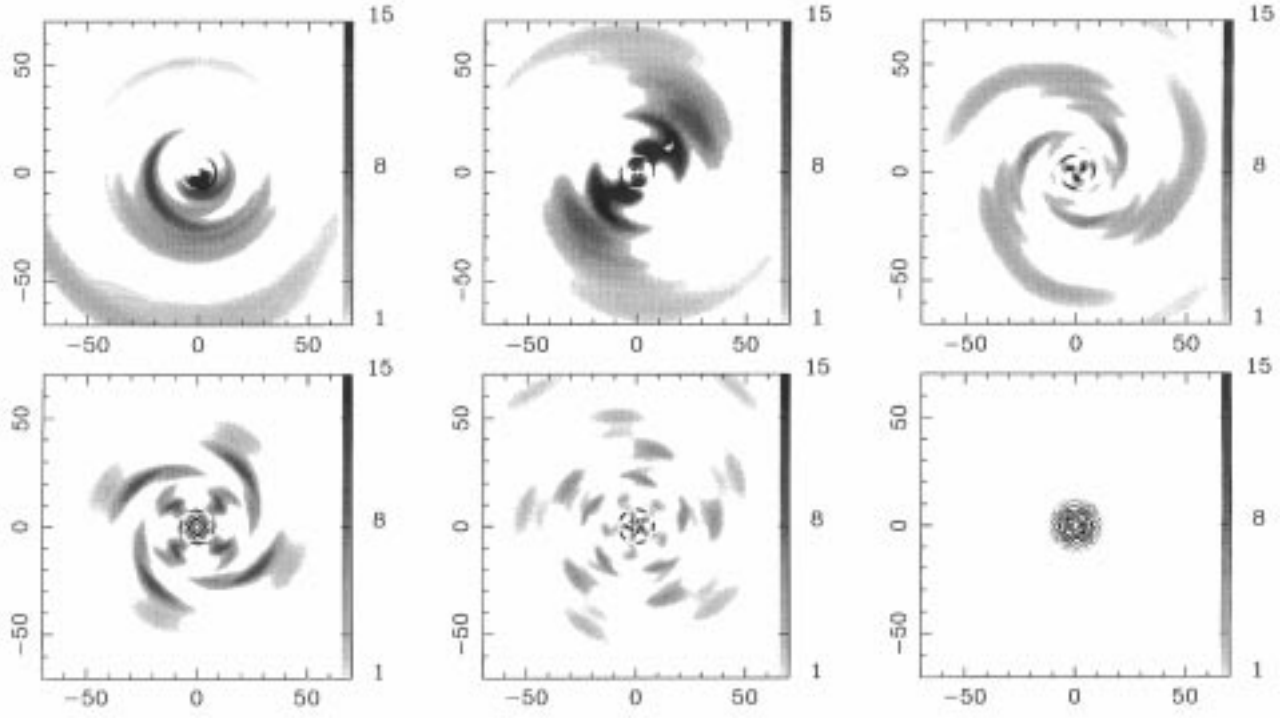

Fig. 2. (continued) Fourier anti-transforms. NGC 7723

4.4. NGC 4321

This impressive galaxy gives the impression of a fantastic whirlpool of light, with two long arms and a large brilliant bulge. Around this can be distinguished four small arms, in principle completely independent of the two main ones. This is the largest galaxy, in relative terms, in our sample, because it is the second closest (beyond NGC 6951) and the second largest (beyond NGC 753). In their H_α study, Arsenault et al. (1988) found an unusual double-lobe structure in the circumnuclear region. They located CR at $\sim 70''$ and the OLR a little further than $128''$, while for the ILR they found found two values, the IILR ($\sim 5''$) and the OILR ($\sim 16''$). Cepa & Beckman (1990b), with higher spatial resolution, determined that this structure is actually an inner spiral which persists after continuum subtraction and that it emits, like the nucleus, in H_α and N II. The corotation radius, predicted by Cepa & Beckman (1990b) from the ILR positions, delimited by the inner spiral arms (the two most prominent of these continue in the main spiral) is $R \sim 80''$, in other words, approximately where dust lanes on concave side of the arms cross over to the convex side (Cepa et al. 1992). From $R \sim 100 - 110''$ the brightness in both arms decreases suddenly, and the number of H II regions too (Cepa & de Pablos 1998).

In the EEM symmetrized images it can be seen that, in general, the best part of the star formation and the B-flux distribution is in the S2 image. In the inner region there is a small spiral, wound in the same sense as that of the two main arms. This structure was observed for first time by Hubble (1934), and is present in all bands. It is a structure with two main arms, which also appear in Fourier transform, and two secondary arms. In the S2 image it seems that two arms extend radially from the nucleus and, from $R \sim 60''$, are "broken" and then turn around galaxian centre. This strange behaviour can be explained by the presence of a very wide bar, which can be discerned in Fig. 4d and which ends at $R \sim 60''$; arms extend from this point. Also we can see that two spiral arms emerge from each tip of this bar. The outermost arms rapidly merge with the bright disc; this suggests that fourth-symmetric components could be very important or even dominant radially, but this cannot be appreciated in the S4 image. The asymmetry in the star formation is very rare. This is shown in Fig. 4d, where, in A2, it is the different sizes of these formation regions that matter, rather than their different locations.

It is not surprising that Fourier transform of this galaxy show a single high maximum in $m = 2$ with $S/N \sim 53$. The other components show a lower S/N ratio and much lower peaks. An exception is $m = 4$, whose peak value is a half that of the $m = 2$ one, and whose $S/N \sim 32$.

The maximum in the $m = 2$ coefficient is centred on $p^2_{\rm max} = 3$, which corresponds to a dominant two-armed spiral with pitch angle $i \sim 34°$. Again, a Gaussian fit changes this result slightly: $p^{\rm g}_{\rm max} = 3.9$ and $i^{\rm g} \sim 27°$. This value is in rather good agreement with that found from a logarithmic fit to the northern arm (Paper III). Other authors find even lower values; Kennicutt (1981), for

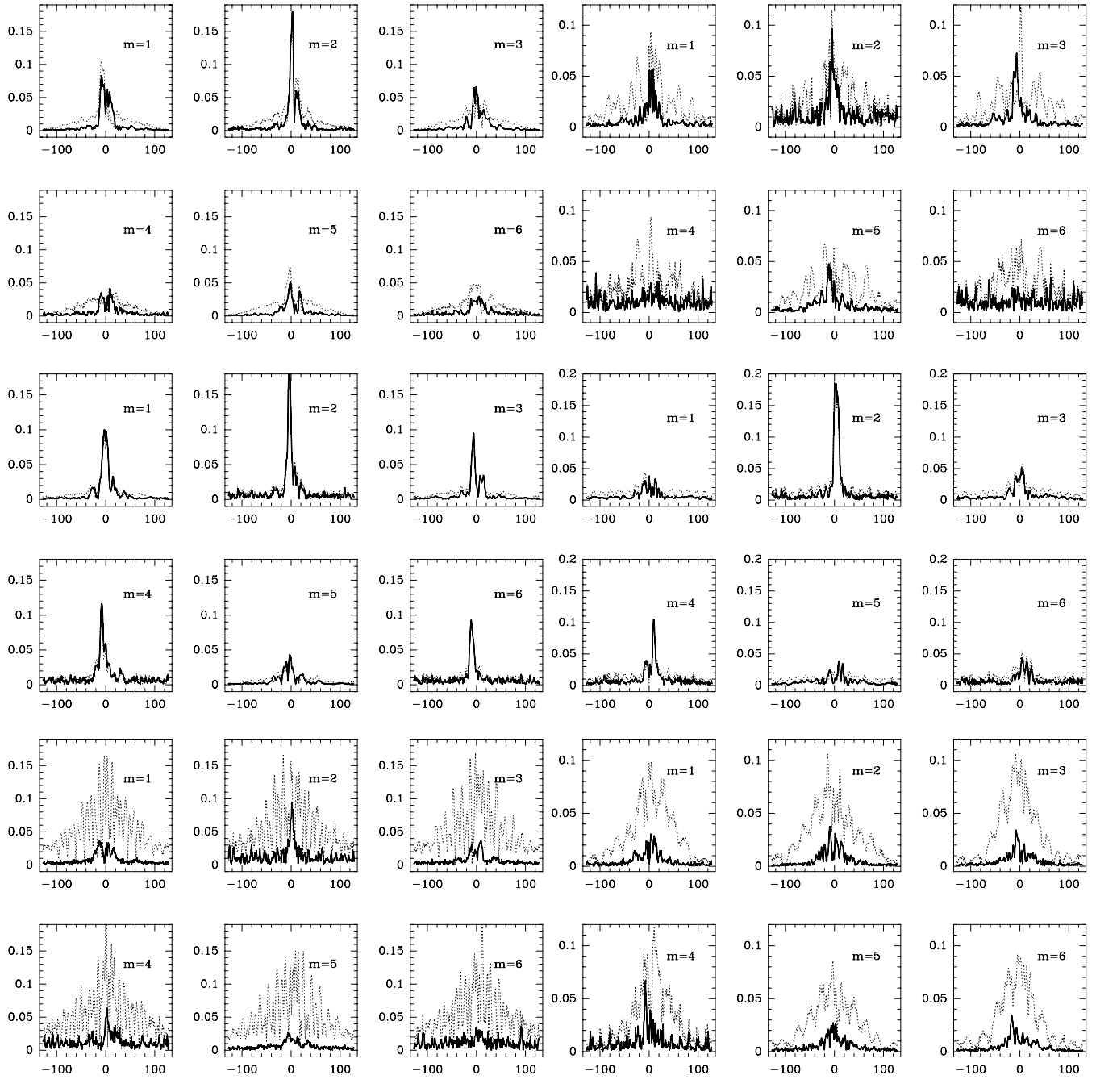

Fig. 3. Amplitudes of $|A(m,p)|$ coefficients. Dotted lines, with field stars, filled lines, without field stars. From left to right and from top to bottom: NGC 157, NGC 753, NGC 895, NGC 4321, NGC 6764 and NGC 6814

example, gives $i = 15° \pm 3°$. Due to the enormous difference between RC3's and Grosbøl's values for the position angle and our value (Table 2), we have used the method of Considère & Athanassoula to calculate the best pair (PA, ω), centred on $(30°, 32°)$, with an interval of $\pm 33°$ between them, so Grosbøl's values are also included. The result was that all 568 pairs have $p^2_{\max} = 0$.

Figure 1d shows the amplitudes of the inverse Fourier transforms for different m values. For $R < 20''$ the components diverge. Over the interval $20'' \lesssim R \lesssim 40''$ all the components are rather similar, and none predominates over the others. That is due to the wide bar, where every component has its own representation (even those that lack importance). In a small fringe ($50'' \lesssim R \lesssim 60''$) $S_2(r)$ has a jump, followed by $S_4(r)$, due to bursts of star formation at the end of the bar. From this point outwards to corotation, $S_4(r)$ is clearly dominant, while $S_2(r)$ decreases even more than $S_3(r)$ and $S_5(r)$.

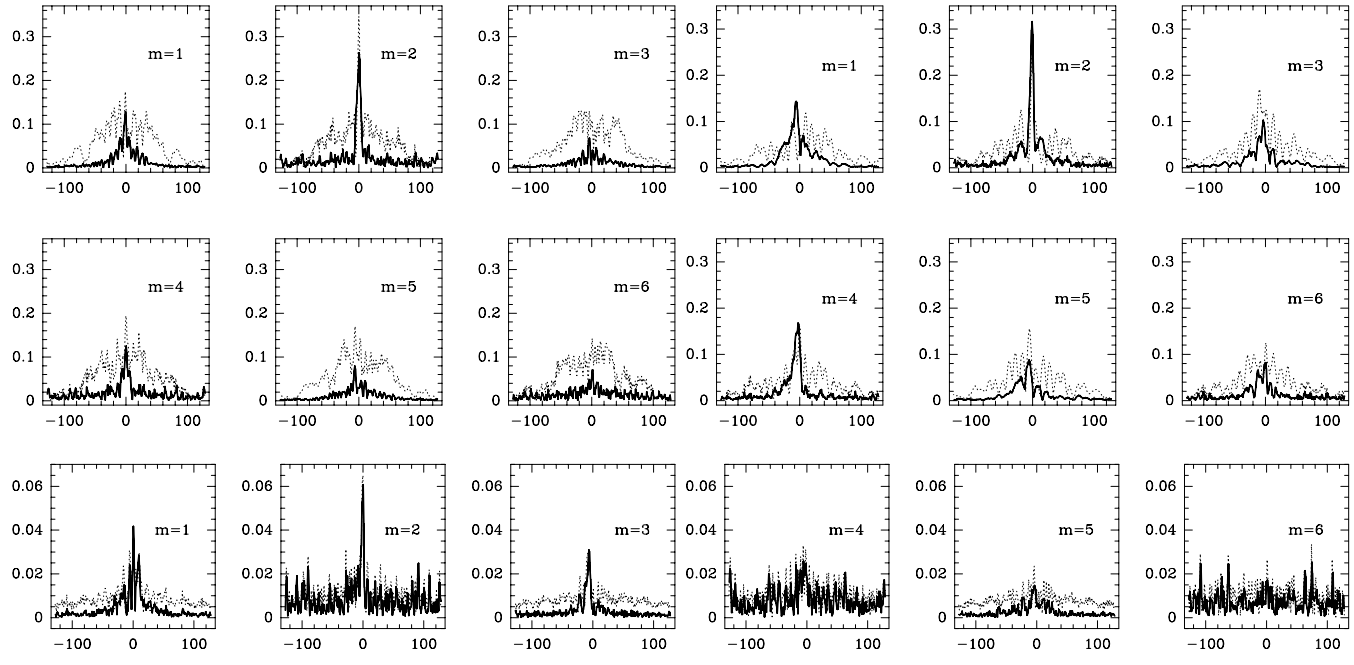

Fig. 3. (continued) NGC 6951 (left), NGC 7479 (right) and NGC 7723 (bottom)

4.5. NGC 6764

This barred galaxy is the first of two Class 5 (Elmegreen & Elmegreen 1987) galaxies that we analyse in this sample. The emission is mainly concentrated in the brilliant nucleus and in two starbursts at the end of the bar. Due to strong optical emission lines in the nucleus, Rubin et al. (1975) classified this galaxy as a Seyfert 2. Later on, Osterbrock & Cohen (1982) obtained a low-excitation spectrum, so they classified it as a LINER galaxy. These authors also found typical emission from Wolf-Rayet stars in the nucleus, which is direct evidence for recent massive star formation. Eckart et al. (1991) measured CO and ^{13}CO emission, as well as obtaining near-infrared (J, H and K) photometry, and calculated an almost linear rotation curve, with a velocity shift between the extremes of the bar of 250 km s^{-1}. The arms emerge from the edge of the bar, and are very short and faint. Before eliminating field stars, all the Fourier transform components are purely noise, with no distinction among them. That is because the signal, when it exists, is below the noise level. Without these stars the coefficients are consistent with those expected in a barred galaxy; the main $m = 2$ component followed by secondary $m = 4$ component. In this case star formation is so rare outside the nucleus and bar extremes that the $m = 1$ component is not relevant at all. The maximum at $m = 2$ is centred on $p^2_{\rm max} = 1$, which corresponds to a pitch angle of $i \sim 63°$. A Gaussian fit shifts this result to $i^{\rm g} \sim 53°$. Even this value is too large for those tiny and almost circular arms. The same problem is present in all the barred galaxies in our sample; the $m = 2$ coefficient is hardly affected by bar emission, which has a pitch angle of 90°, so the pitch angle derived from $p^2_{\rm max}$ gives an idea of the relative importance of the bar versus the arms, more than the real arm shapes. Looking at bi-dimensional distribution of the Fourier coefficients, it is evident that S_2 is the only important component, and that S_4 contains information on both the arms and the bar, but not on the four-armed structure. The most striking feature of Fig. 2e is that the winding sense of S_1 is contrary to that of the main modes, S_2 and S_4. If, as Pasha (1985) asserts, the galaxy is *trailing*, then this means that it contains a *leading* component. The phenomenon is not new, even though it is rather infrequent; Considère & Athanassoula (1982) found both *trailing* and *leading* arms, represented by different modes, in a certain galaxy. For $R \gtrsim 65''$, where there is a local minimum in $S_2(r)$, emission of all the components drop (except for $m = 1$, which falls at $R \sim 70''$, but this is due to a field star that we could not remove because it is too close to the end of one of the arms). The radius at 25 μ is also $R \sim 65''$. If this is the OLR, as claimed by Elmegreen & Elmegreen (1995), and the rotation curve is locally flat (Eckart et al. 1991), then corotation should be at $R \sim 30 - 31''$, coinciding with the deepest local minimum of $S_2(r)$. But this radius is *inside* the bar (which reaches $R \sim 37 - 40''$), and we have not studied this range in Paper III. Instead, we have found outlines of change in skewness and different mean position signs at $44'' \lesssim R \lesssim 47''$. This range corresponds to a local minimum in $S_2(r)$ and a change in dominant mode (from $m = 2$ to $m = 4$). If corotation falls between these values, the OLR should be at $94'' \lesssim R \lesssim 100''$, too far away, taking into account the galaxian dimensions.

We cannot reach any conclusions concerning the resonances in this galaxy by any method. The arms are much too faint in our image to distinguish different features away from the bar; they are also intrinsically faint, as the very low amplitude in the I band demonstrates (Paper III).

4.6. NGC 6814

This is a clear exception in our sample, it is a grand design spiral with a four-armed dominant pattern. The visual appearance of multiple arms is confirmed in the Fourier decomposition. Beyond $R \sim 18''$, where its bright nucleus is dominant (it is a Seyfert 1 galaxy, Ulrich 1971), the $S_4(r)$ component is stronger than the others, included the $S_2(r)$ component. Perhaps due to this anomaly the arms die out at corotation, as derived from spiral density wave theory (first because with $m = 4$ the range of existence is shorter, and secondly, because *leading* waves die at CR).

This is the galaxy with least inclination in our sample, only 7° (Grosbøl 1985; Paper II) although other authors give higher values (21°, de Vaucouleurs et al. 1991; hereafter RC3). This Seyfert 1 galaxy has strong H_α emission (Knapen et al. 1993). The nuclear region dominates the total emission. The low inclination of this galaxy permits us to appreciate more easily that the arms trace the disc. As they go further from the nucleus, the two arms that emerge from it begin to bifurcate several times, that gives a multi-armed aspect to the galaxy. The brightest arms complete approximately one revolution up to $R \sim 49''$. From this radius, their luminosity decays abruptly, ending at $R \sim 65''$. Dust seems to be present in a weak but constant manner, mainly on the convex sides of the arms, out to $R \sim 21 - 27''$, where it crosses them for the first time. Several more crossings are seen, but dust is not conspicuous on the concave sides of the arms.

Fourier decomposition with field stars is very noisy (as in the case of NGC 6764). When cleaned, the signal is very low, in fact the maximum is at $|A(4,p)|$, with an intensity of only 0.065. This is the only case in our sample where $|A(2,p)|$ is not the most important coefficient. It is worthwhile noting that the intense peak in Fig. 1f is due to a field star over the southern arm, so all bi-dimensional distribution images are affected by it.

Except for the very inner regions ($R \lesssim 18''$) where $S_2(r)$ is the principal component, the image is dominated by a four-armed pattern, with an important $S_3(r)$ contribution (see Table 1).

Corotation is presumably at $R \sim 45''$ (Paper III) close to an $S_4(r)$ local minimum. As we have already mentioned, this is the only case where we do not find a two-armed pattern dominating the morphology of a galaxy; it is also the only case where, in our previous work (Paper III), we found a *leading* dynamical pattern. NGC 6814 has no companion which can induce *leading* arms, as Pasha (1985) found in every *leading* galaxy in his study. These peculiarities could be just a coincidence, but it is more probably that the phenomenon which inhibits *leading* behaviour in spiral galaxies is related with a mechanism that encourages the formation of two main arms. If this is true, the absence of such a mechanism permits the presence of four-armed *leading* patterns.

This is an exception in our sample, it is the only case where a grand design spiral has a dominant four-armed pattern. The visual appearance of multiple arms is confirmed in subsequent Fourier decomposition. Although this is not a conclusive proof, it confirms the spiral density wave theory prediction that *leading* waves, both short and long, end at CR, even when the four-armed pattern could extend up to the 4:1 OLR, theoretically at $R \sim 70''$.

4.7. NGC 6951

This is a galaxy whose major emission is concentrated in a bar-like structure; in fact it has been classified as both S and SB in different catalogues (RC3; Sandage & Tammann 1987). This structure, together with two relatively weak arms, make the Fourier method of finding optimal values of PA and i difficult because $p^2_{\max}$ values are always centred on 0.

This galaxy has the characteristics of barred and normal spirals. It is a clear example of transition between to "pure" types of spirals. Several prominent dust lanes are visible, one of these originating in the central region. The bright bulge is elongated in the direction of this dust lane, almost perpendicular to the major axis. The arms are relatively short (around 180°), the most symmetric part ending approximately at $R \sim 100''$ and extending somewhat beyond some starbursts. The arms are considerably fainter than in the other *grand design* galaxies in the sample.

The $|A(2,p)|$ coefficient is, without doubt, the most important in the Fourier decomposition, with a unique and very pronounced peak ($S/N \sim 32$), as is expected in the case of barred spirals. Second in order of importance is $|A(1,p)|$, ($S/N \sim 16$) and finally, $|A(4,p)|$ ($S/N \sim 15$). The other components ($|A(3,p)|$, $|A(5,p)|$, and especially $|A(6,p)|$) are essentially noise, without significant peaks. A substantial improvement is appreciated in all the coefficients when field stars are eliminated.

As with NGC 6814, the $|A(4,p)|$ coefficient presents a series of peaks which are symmetric with respect to $p = 0$; this is the reason why the signal-to-noise ratio is much lower than would be expected from Fig. 3g. The maximum of $|A(2,p)|$ is at $p^2_{\max} = 0$, with and without field stars, which corresponds to arms that extend radially from the nucleus. This could be due to the deprojection not being completely correct, or, more probably, to the influence of the bar, which dominates the Fourier transforms in the same way as the images obtained by the EEM method.

Table 3. Summary of correlations between change of modes and minima in dominant modes at or around corotation for the galaxies of the sample. NGC 6814 has been excluded since its arms end at corotation

NGC	Bar	AC[1]	CR (″)[2]	Change of dominant mode	Minimum (″)[3]
157	No	12	40	No	40
753	No	9	30	From $m = 2$ to $m = 3$ at 40″	28
895	No	9	75	From $m = 2$ to $m = 4$ between 75″ and 80″	77
4321	Yes	12	80	From $m = 4$ to $m = 2$ at 80″	
6764	Yes	5	30/45?	No	33
6951	No	12	70?	No	
7479	Yes	9	85	From $m = 2$ to $m = 1$ at 80″	85
7723	Yes	5	35	From $m = 2$ to $m = 4$ between 30″ and 35″	27

[1] Arm class according Elmegreen & Elmegreen (1987).
[2] Corotation determined in del Río & Cepa (1998b).
[3] Minimum nearest to corotation in the dominant mode.

A Gaussian fit to $|A(2,p)|$ does not vary the results substantially ($i^{\rm g} \sim 77°$). The lack of a symmetric arm in the one studied provokes this behaviour in transforms. Obviously, the dominant component is $m = 2$, but it does not account for the arms in the same way that the EEM method fails to do. There is an arm that is clearly dominant over the other one, and this is shown in Fig. 2g, where we see the bar and the incipient arms S2, as in S2; S_1 show the strongest arm, which is more active in terms of star formation. Finally, in S_4 a feature common to all spirals with a strong bar can be seen: the "arms" are spurious and are really a consequence of the flux between the wide bar and the main arms. The maximum of the $|A(1,p)|$ coefficient is at $p^1_{\rm max} = -1$, which leads to a pitch angle $i \sim 45°$ ($i^{\rm g} \sim 43°$), in reasonable agreement with that found for logarithmic fits to the main arm (Paper III). This confirms that our initial deprojection was correct. The result is not improved either with Considère & Athanassoula or the Puerari & Dottori method. The latter yields similar PA and ω values (although somewhat higher for ω), and the same value for i, but the convergence (see Fig. 7) is not very good. The first gives a bad convergence (Fig. 6), low signal (Fig. 8) and high dispersion between the observed and fitted pitch angles. The value found in Paper III falls between these.

The corotation radius is not clearly defined, although all the evidence points to $R \sim 70''$ (Paper III). Nothing special occurs at this radius in $S_2(r)$, but it seems to be the end point of $S_1(r)$.

In the bi-symmetric image, the arms dilute in the disc at $R \sim 75''$; nevertheless, in A2 we can follow their faint trace until the limit of the frame, i.e. $R \sim 150''$, which could correspond to the OLR. This value is in reasonably good agreement with that found theoretically ($\approx 152''$) assuming a locally flat rotation curve and a corotation radius of $R \sim 70''$. In A2 there is also present a ring around the nucleus, slightly shifted forward by 90° in the image ($\sim 257°$ in the original frame), with a radius $R \sim 9''$. This singularity corresponds to the (theoretical) ILR, with the same assumptions as before.

4.8. NGC 7479

This is another important barred galaxy in the sample, but the main difference from the former galaxy is that in this case there is a strong blue arm, which has a pitch angle rather similar to that found with a simple least-squares fit.

This galaxy has been identified as a starburst type with moderately wide CO lines (Young & Devereux 1991). This barred spiral shows a weak continuum in its nucleus, with faint H_α and [N II] emission, whereas in the bar it is stronger. The H_α line shape implies the presence of large and brilliant H II regions along the bar (Hua et al. 1980). At the end of the bar, which is 100″ long, two arms originate; one of these is bifurcated even before it leaves the bar. This effect, probably an optical one, may be caused by a dust lane accompanying the east-north arm to its end. The west-south arm, much more regular, is also accompanied by a dust lane, but which is shorter than the other one, because it finishes near the supernova remnant of SN 1990V, at $R \sim 60''$.

The coefficient $|A(2,p)|$ shows the highest maximum in our galaxy sample, ∼40% larger than the same coefficient for NGC 6951, the other "intense" barred spiral in the sample. Although the noise in all the coefficients diminishes notably when field stars are removed, ($|A(2,p)|$ goes from $S/N \sim 18$ to $S/N \sim 71$, and $|A(1,p)|$ from 8 to 48), only the maxima of the secondary components ($|A(3,p)|, |A(5,p)|$ and $|A(6,p)|$) vary. The maximum of $|A(2,p)|$ is at $p^2_{\rm max} = -1$, which corresponds to $i \sim 63°$, much higher that found in Paper III. A Gaussian fit gives $i^{\rm g} \approx 49°$, which is closer to the value calculated for the first part of the arm (before corotation). Calculation with the Considère & Athanassoula and Puerari & Dottori methods does not improve the results. From Fig. 2g it is not difficult to understand why the pitch angles are so high; the bulk of the image is in the bar, whose pitch angle is 90°.

A second important maximum occurs in $|A(1,p)|$ (S_1 represents the outer part of the arms, in particular the western arm), with $p^1_{\rm max} = -6$, i.e. a pitch angle

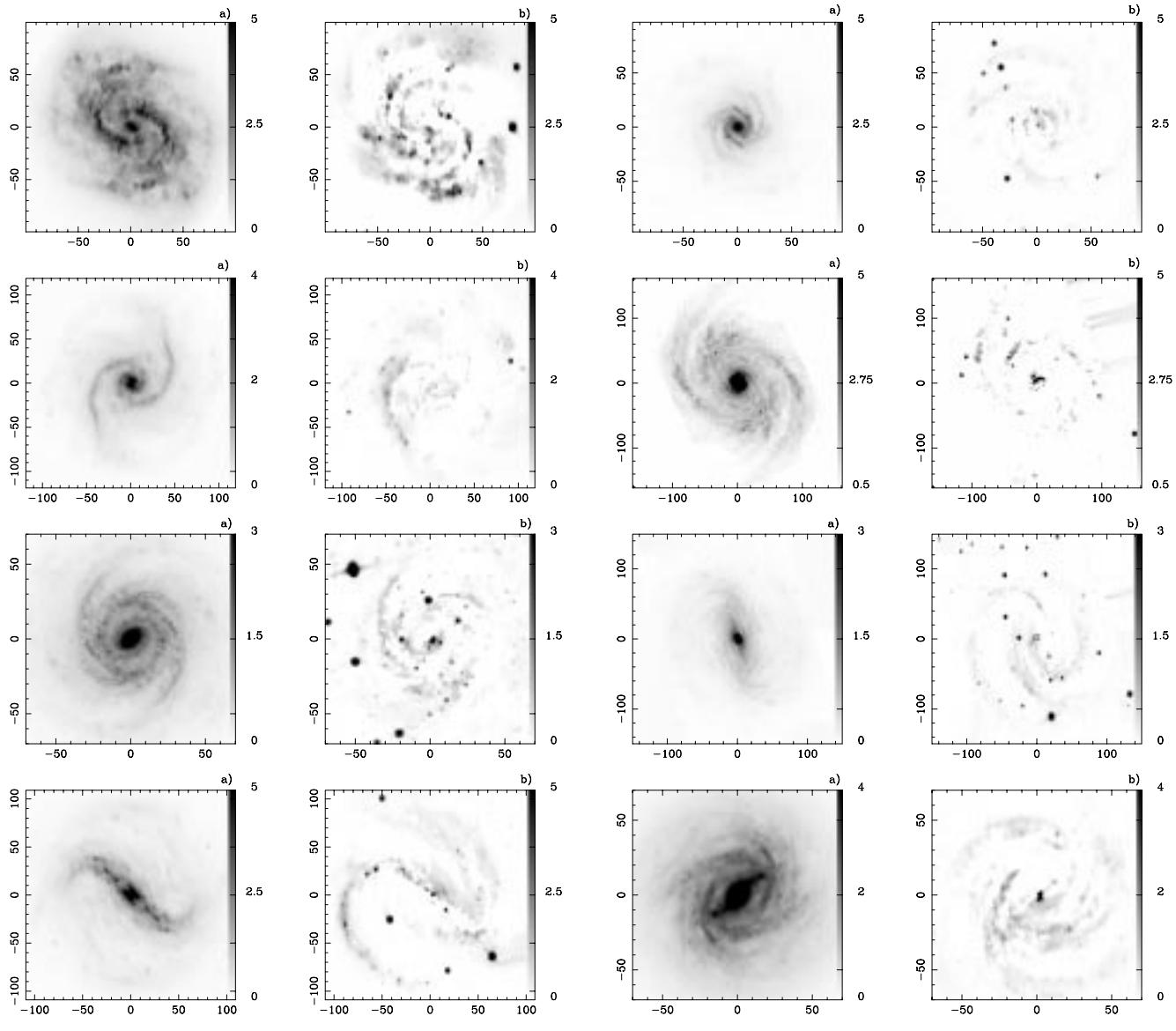

Fig. 4. Symmetric and asymmetric images from the EEM method. From left to right and from top to bottom: NGC 157, NGC 753, NGC 895, NGC 4321, NGC 6814, NGC 6951, NGC 7479 and NGC 7723

$i \sim 10°$, somewhat lower than calculated by Paper III for the outer arm (after corotation). This is because arms become circular ($i \sim 0$)) at $R \sim 90''$, so that azimuthal profiles cannot be computed and the fit must be performed over a range smaller than that of the Fourier transform. In addition to the bar, two small arms, with different pitch angle, can be seen in S_2 (Fig. 2g). Their origin (which marks the tip of an intense emission) matches with an $S_2(r)$ minimum and a change in dominant mode (from $S_2(r)$ to $S_1(r)$). In fact, all the components exceed $S_2(r)$ in an interval around $R \sim 85''$, but $S_1(r)$ is dominant until the end of signal.

With the EEM method we see also that all symmetry is in the bar; not even the bulge is symmetric (a part appears in A2). The unusual symmetry of this galaxy is reflected in S2, where there is only 69% of the total emission, much less than in other *grand design* galaxies, despite the bright bulge and the star formation zones in the bar. The short arms visible in S2 hardly reach $R \sim 65''$, far away from corotation. In fact, there is no appreciable change at $R \sim 85''$. This is mainly due to the absence of a clearly defined second arm for $R > 65''$, which eliminates, in the symmetrizing process, any indication of the western arm.

In Paper III we established that corotation is at $R \sim 85''$, where we found changes in the skewness signs, both in the B and I bands, and in pitch angle, showing that the arm is "broken". With the Fourier transform method we now find more evidence that supports our former

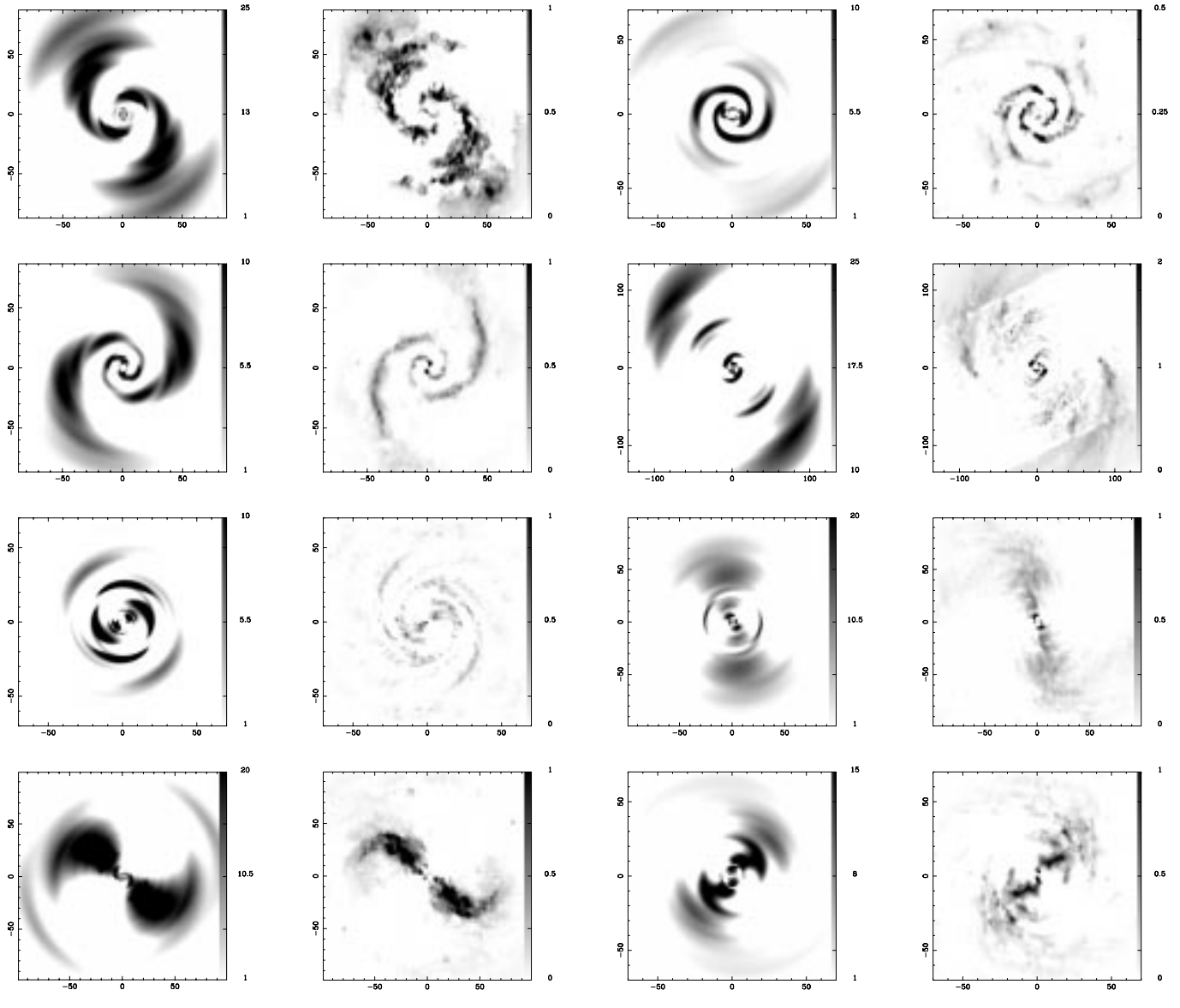

Fig. 5. Comparison between S_2 (left) and $S_2 - S_4$ (right) images. From left to right and from top to bottom: NGC 157, NGC 753, NGC 895, NGC 4321, NGC 6814, NGC 6951, NGC 7479 and NGC 7723

result, such as a local (and global) minimum in the main component, $S_2(r)$, local maxima of the other components and a change (in this case, definitive) of dominant mode.

4.9. NGC 7723

This galaxy, as occurs with NGC 6764, is Class 5 (Elmegreen & Elmegreen 1987), i.e. its arms are less defined than in the other galaxies. It can be seen that the arms are two faint small outlines that originate at the end of the bar and very soon bifurcate. One part (of each pair) is closed around the nucleus, and the other part is partially opened on the outer side. The "inner" arms form an almost complete ring around the small bar.

Figure 4h shows a galaxy with a prominent bulge (8.4 kpc) and a bar 40″ in length that dominate the S2 emission, which contains 90% of the total flux. The high percentage is not due to the arms, which are relatively short and faint, but to the bulge and bar. The asymmetric image, in addition to part of the bulge, contains "three" moderately intense arms. Two of these correspond to the outer main arms and the third, the most open, one to the prolongation of one of the secondary arms. The high degree of symmetry could be due to a density wave generated by the bar, with a very low intensity, insufficient to trigger significant massive star formation processes along

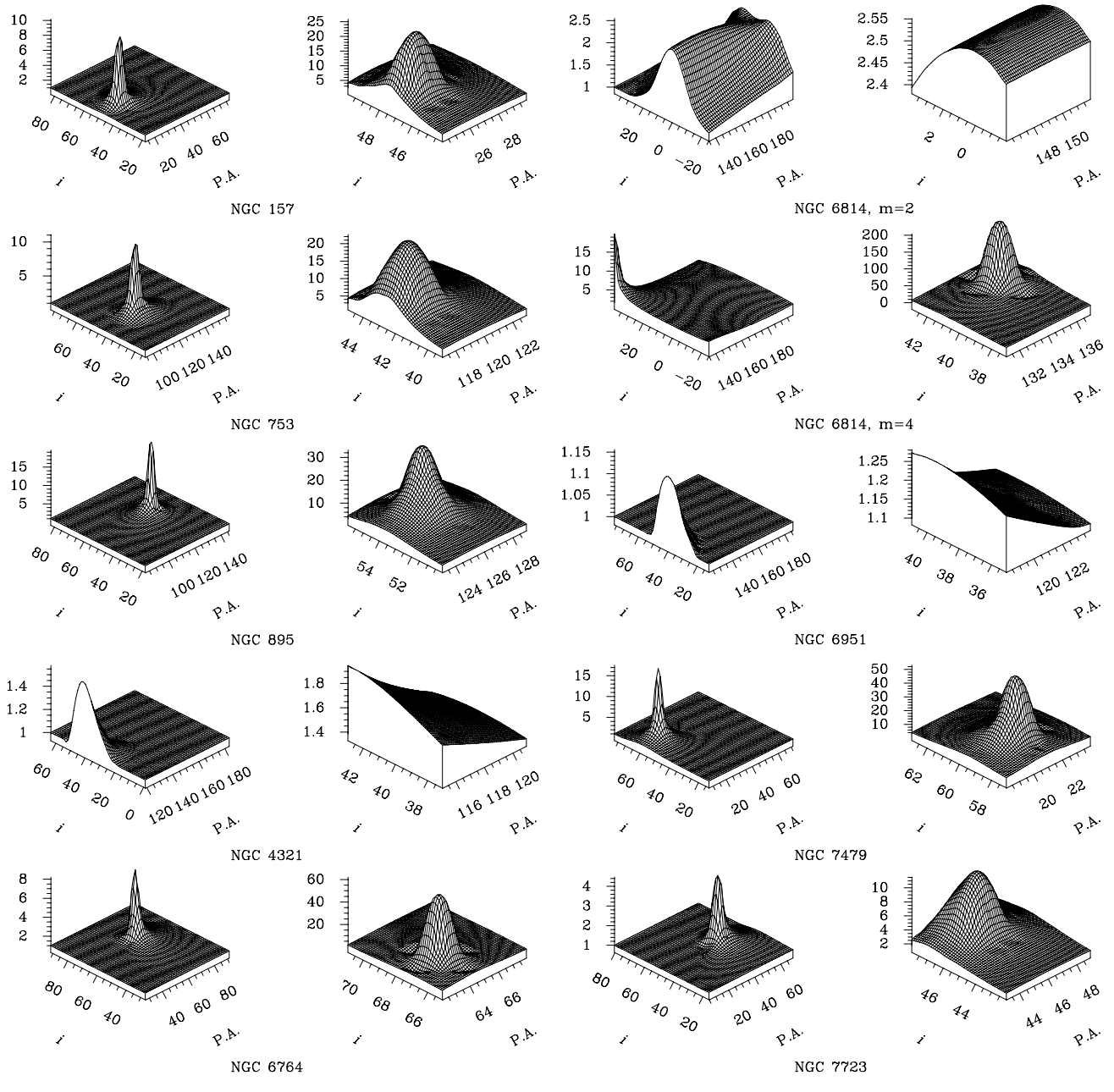

Fig. 6. Convergence of angles with Considère & Athanassoula method

a very well defined spiral structure. The brightest part of S2 ends at $R \sim 35''$, where the sign of the difference in mean position changes (Paper III), while the arms in A2 are brighter from this point.

In contrast with the other galaxies, S3 has a relatively important weight in the structure of this galaxy. There is a ring in S3 at $R \sim 20''$. Corotation was not firmly defined in Paper III, but the difference in mean position, in one arm and the end of the brightest part in the other point to $R \sim 35''$ as a possible corotation radius. In this case, $R \sim 20''$ corresponds to the 4:1 ILR. The second (Schwarz 1984) is in this resonance where rings are formed when bars are not very strong.

The Fourier coefficients are noisy and faint, even $|A(2,p)|$ which, as for all barred galaxies, presents a sharp high peak, although of very low intensity (lower than the $m = 2$ peak of the other class 5 galaxy, and comparable only to the $m = 4$ maximum of NGC 6814). Also, as for almost all barred galaxies, $p^2_{\max} = 0$, and with a Gaussian fit pitch angle change to $i^{\rm g} \sim 63°$, still too much large for some small, tightly wound arms.

Unlike NGC 6764, this galaxy has a rich Fourier structure. Figure 2h is dominated by the image of S_2, which contains the bar and the brightest part of the arms. S_3 also has a clearly defined structure, which corresponds to the three brighter inner arms, and their continuation, much

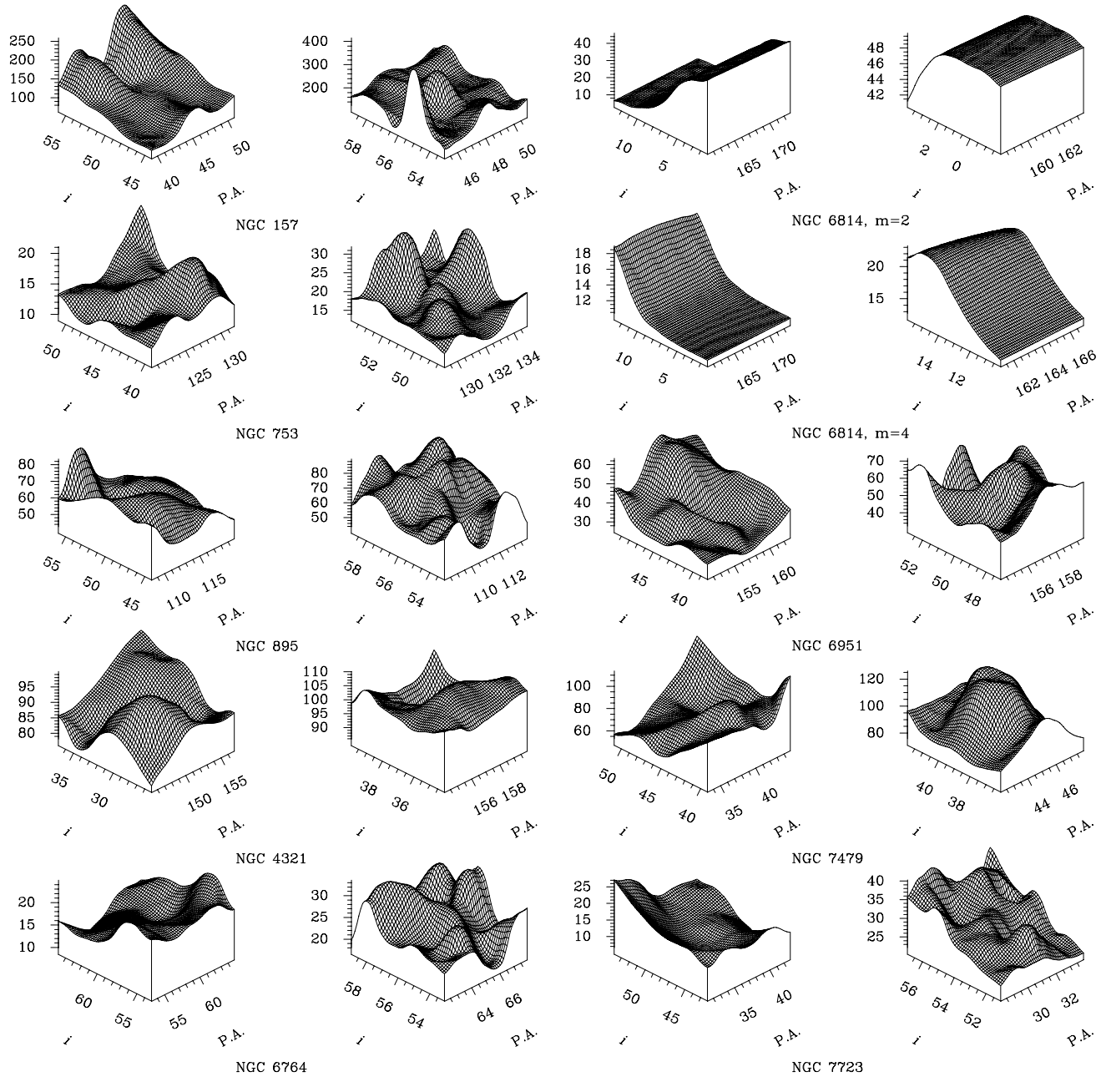

Fig. 7. Convergence of angles with Puerari & Dottori method

more open and faint, out the edge of the disc, with a pitch angle $i_3 \sim 20°$, similar to that found by Paper III.

The ring already mentioned appears in S_1 and S_3 (incomplete in each frame, but nearly closed in the S_1+S_3 image). The S_4 component dominates S_2 in a small interval around corotation. At $R \sim 50''$ (the 4:1 outer resonance) S_3 becomes higher than S_2, out to $R \sim 58''$ ($\approx$ 3:1 outer resonance). The OLR, at $R \sim 70''$, marks the point at which the secondary components definitively overcome S_2.

In summary, no result, separated from the global context, is conclusive concerning CR, but all the results together lead us to the conclusion that CR is effectively located at $R \sim 35''$.

5. Conclusions

The Fourier transform method provides us with a natural way of studying the different symmetries inside a galaxy. Spiral arms are quite well approximated by logarithmic spirals, so with a very few terms (usually two or three, and never more than four) it is possible to reproduce the structure and main features of galaxies, without losing

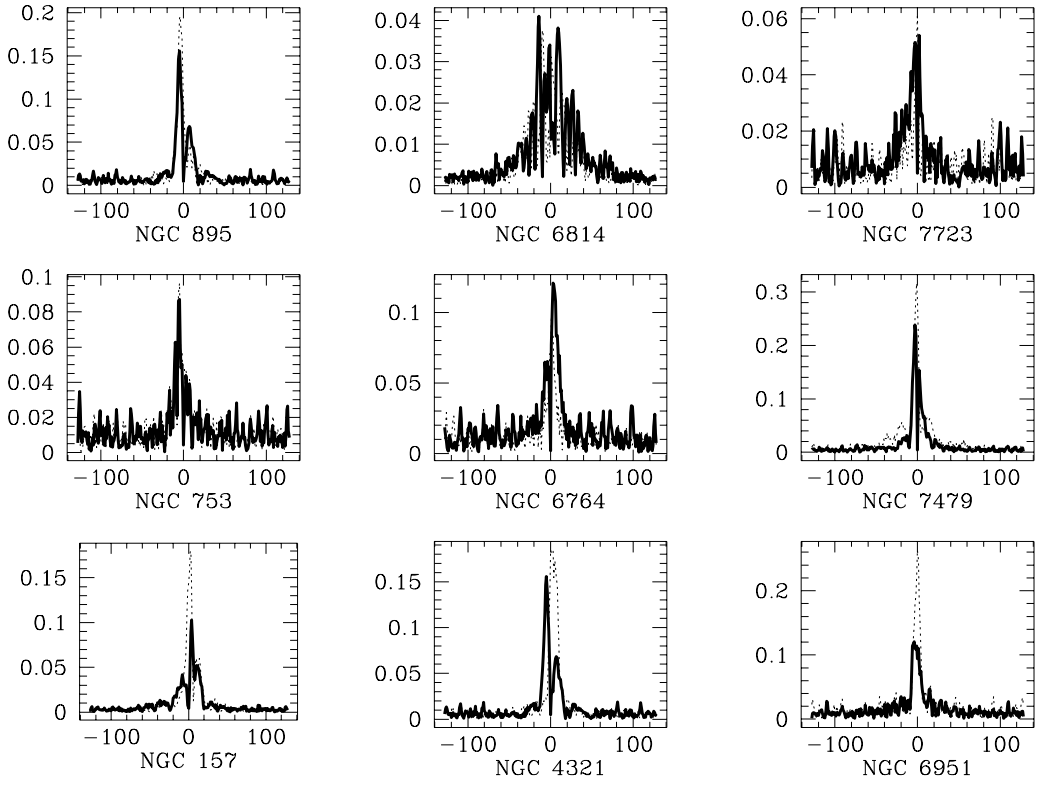

Fig. 8. Comparison of $|A(2,p)|$ coefficients found with the Considère & Athanassoula method for the best pair of angles (PA, ω, thick line) and our values (dotted line)

Table 4. Pitch angles calculated from Considère & Athanassoula method (marked with CA), from Puerari & Dottori method (marked with PD) and from our work (marked with OW). All values have been found with $m = 2$ as main component, except those marked with †, that have been calculated with $m = 4$ dominant mode

Object	$i_{\rm CA}$	$i^{\rm g}_{\rm CA}$	$i_{\rm PD}$	$i^{\rm g}_{\rm PD}$	$i_{\rm OW}$	$i^{\rm g}_{\rm OW}$
NGC 0157	26°	28°	45°	63°	34°	24°
NGC 0753	22°		90°	53°	22°	27°
NGC 0895	22°	21°	22°	38°	26°	29°
NGC 4321	16°	24°	90°	36°	34°	27°
NGC 6764	33°	30°	33°	37°	63°	53°
NGC 6814	8°	51°	63°	51°	40°	11°
NGC 6814†	26°	84°	26°	18°	26°	68°
NGC 6951	26°	53°	90°	78°	90°	77°
NGC 7479	33°	57°	90°	59°	63°	49°
NGC 7723	45°	20°	45°	78°	90°	63°

three-dimensional information. It is also possible to quantify the relative importance of each component for a prefixed radial interval. With $S_m(r)$ functions we can easily locate maxima and minima, and relate them with different resonances, where these exist, but the most important application we have found is that, with these functions, the change of dominant symmetry near or at corotation is (very) clear.

In all cases where corotation was clearly defined (Paper III) the Fourier transforms have confirmed this radius. In cases where corotation was not so firmly established, Fourier transforms have helped to locate different features, such as rings, breaks, changes in dominant mode, etc., and with these it was possible to find a reliable value for this resonance. Although corotation does not in all cases match a local minimum in $S_2(r)$ (or $S_4(r)$ in NGC 6814), it is usually close to one of them, close to maxima of secondary components (generated by the stochasticity of stellar orbits at this point), or close to a change in dominant mode, etc. With this information we have confirmed (or discarded) the location of corotation and the other main resonances.

Both methods (Considère & Athanassoula's and Puerari & Dottori's) have serious drawbacks in calculating the best pair of angles (PA and ω) for a galaxy.

The Considère & Athanassoula method converges quite well to a pair of values, except for NGC 6814, where any PA is equally good, because the galaxy is almost face on, and NGC 6951, where the ratio $|A(2,p)|/|A(0,p)|$ is

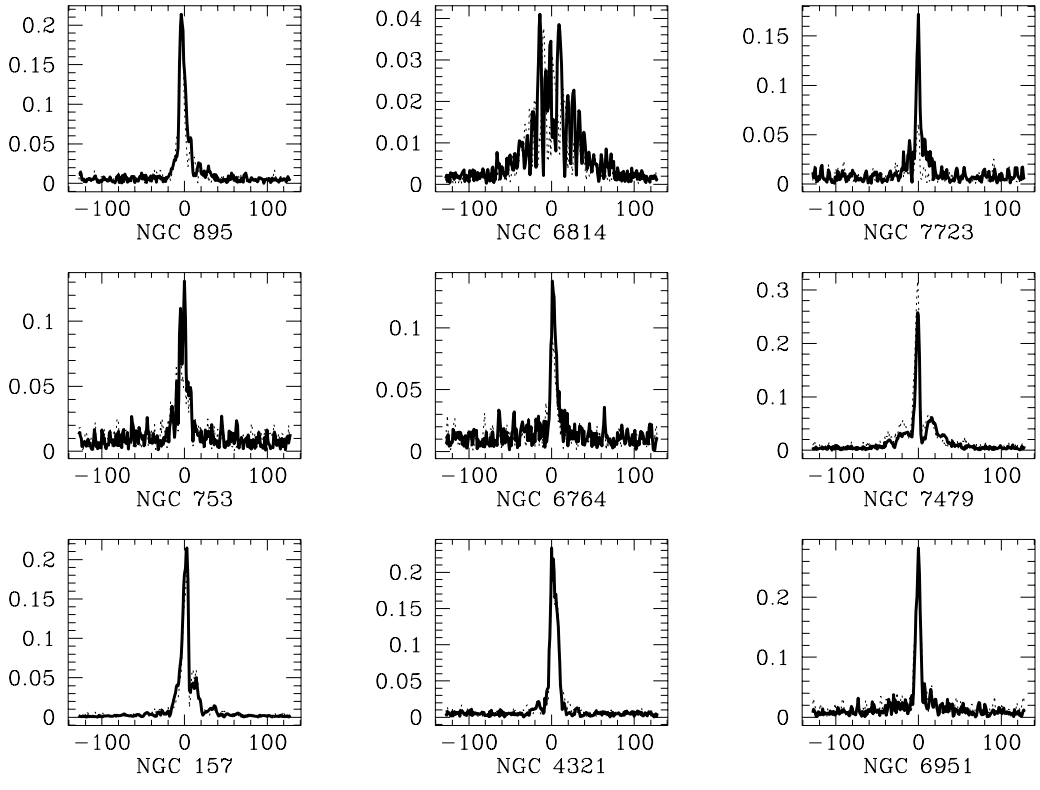

Fig. 9. Comparison of $|A(2,p)|$ coefficients found with the Puerari & Dottori method for best pair of angles (PA, ω, thick line) and our values (dotted line)

not very high (it is strong barred, so $p^2 = 0$ is important in any deprojection). But this pleasing convergence, which can be seen in Fig. 6, is somewhat spurious. If we represent the new $|A(2,p)|$ coefficient vs. that calculated with our PA and ω values (Fig. 8), we can see that in the majority of cases the amplitude is lower (i.e. the arms are "less" logarithmic) and the reason why the ratio is so high is because only the point with $p = 0$ has a very low amplitude, close to zero (among 568 pairs the probability of finding such a case is finite). Furthermore, when galaxies are strongly barred and have faint arms, the correct deprojection could lead to $p^2_{\max} = 0$, due to the influence of the bar. In this case this method also fails, because it chooses the first pair of values with $p^2_{\max} \neq 0$.

The Puerari & Dottori method has the opposite problem: while coefficients have a "normal" shape (i.e. they do not have a gap in $p = 0$) and in some cases are even higher than those calculated previously (Fig. 9), as is the case, for example, of NGC 7723, with more than twice the new amplitude, the convergence is worse (Fig. 7). It also presents the problem that galaxies with strong bars and faint arms have a very important contribution at $p^2 = 0$, which is strongly favoured when the deprojection, even if wrong, is "aligned" with the bar; i.e. when the new major axis is almost perpendicular to the bar. This is a cumulative effect. When the deprojection is wrong, with inclination angles larger than the correct value, the isophotes are elongated in the $\widehat{y}$-axis; hence, if the bar is also aligned with the $\widehat{y}$-axis, by varying the position angle the p^2 coefficient can reach values very close to zero. In this case also, the outer isophotes are not circular with the new deprojections.

Finally, both methods have the same problem in that they both optimize the best "view" of a galaxy to obtain the most perfect logarithmic arms. This works only for a very few galaxies, such as NGC 895, which has two long bi-symmetric arms (Fig. 5 and Fig. 2), whose fit to a logarithmic spiral is exceptionally good (Paper III). But this is not generally the case: logarithmic arms are only an approximation, and are not good enough when arms multiply or bifurcate, when one arm is much brighter than the others, when the pitch angle changes due to processes at corotation, etc. In such cases, both methods present a view of the galaxy which is not real or correct. Even the outer isophotes cease to be circular with these deprojections, and we think that it is much more physically plausible

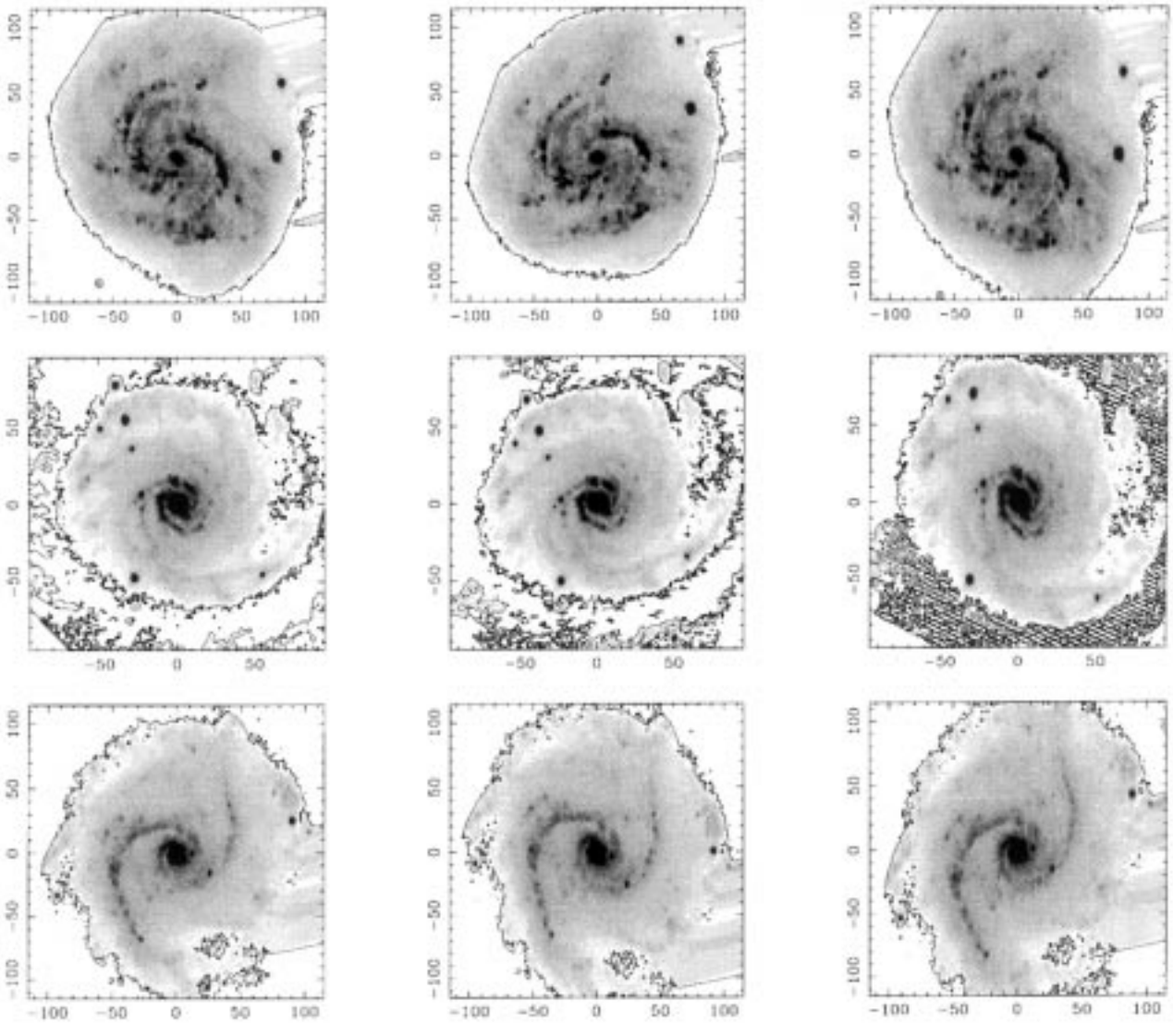

Fig. 10. Different projections. For each galaxy, with values found in Paper III (left), with those found with the Considère & Athanassoula method (centre) and with those found with the Puerari & Dottori method (right). From top to bottom: NGC 157, NGC 753 and NGC 895

that the outer isophotes are almost circular than that the arms are perfectly logarithmic.

We have not found any relevant tri-symmetry component (except in NGC 7723) with the EEM method, much less four-symmetric components, even in those cases where Fourier transforms of such degrees dominate the S_2 image. This could be because different symmetries are mixed in the same image, while the Fourier transform method separates better the different components. Figure 5 shows a graphical comparison between the S_2 and S2−S4 images, demonstrating that symmetry separation is performed in a different way with each method. With the Fourier transform, points with a fixed flux that appear twice and only twice in the image are kept, whereas with EEM symmetrization, points that appear two, four, and presumably any multiple of two, times remain in the result, thereby smoothing the contrast, and do not allow the characteristic features of the bi-symmetric image to be found. We have not performed the symmetrization beyond S4, so we cannot assert that the same occurs with S3 and S4 images, but this is probably the reason for the lack of information on these images, which can be easily appreciated in S_3 and S_4. When there is a strong, or a wide bar, the FT component $m = 4$ is "artificially" enhanced, as pointed by Elmegreen et al. (1993). This is the case for NGC 6951 and NGC 7479. Other barred or pseudo-barred galaxies in the sample do not show this behaviour. But even in those cases, $m = 4$ (or higher modes) is note the dominant component in the relevant part of the galaxies.

It is tempting, as is commonly done, to associate the flux minima to resonances (as Elmegreen & Elmegreen did in 1995), but this idea can lead to confusion. In some cases

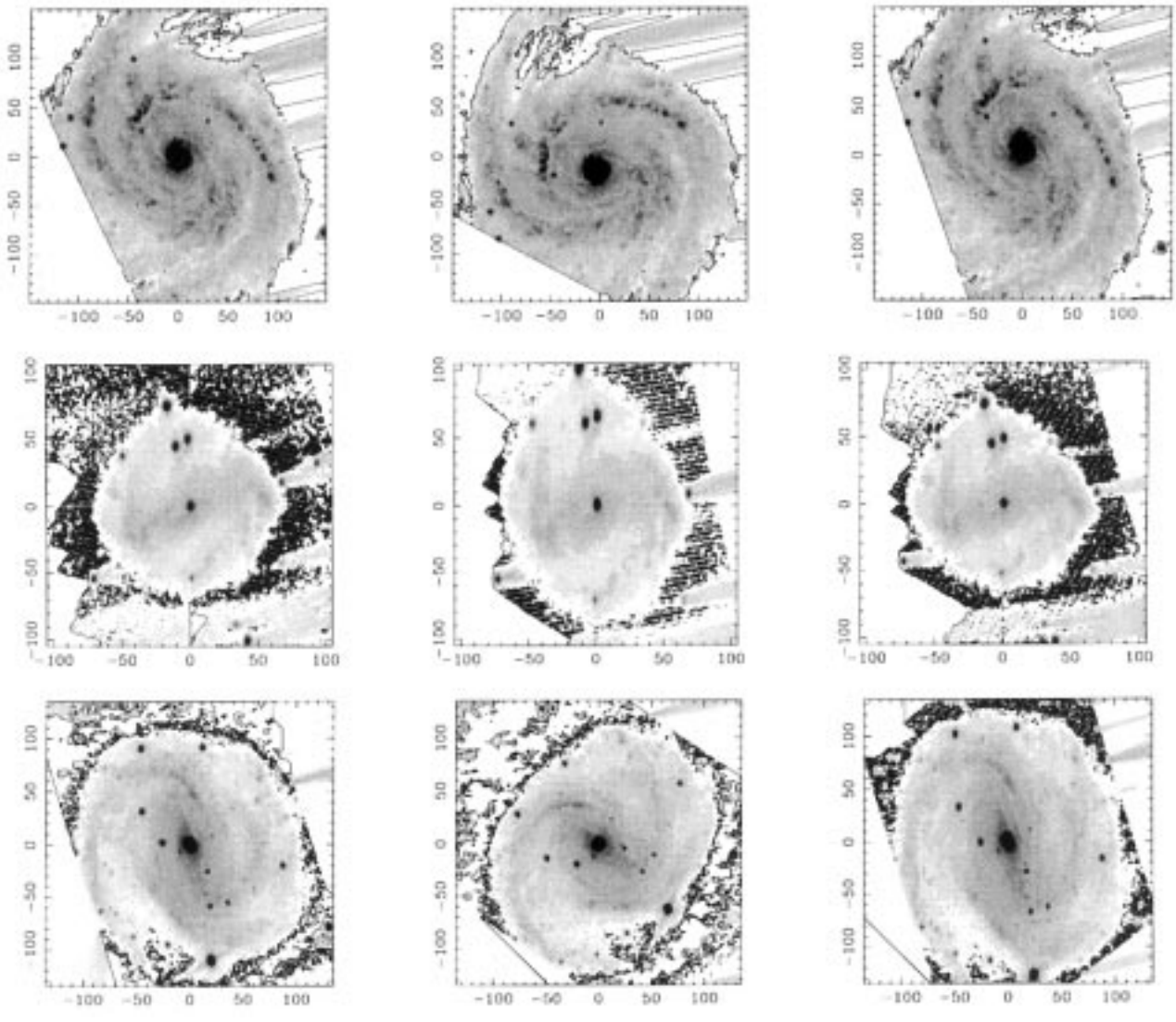

Fig. 10. (continued) From top to bottom: NGC 4321, NGC 6764 and NGC 6951

the brightest arms end near corotation (e.g. NGC 7479 and NGC 6951), but in others they are longer (NGC 895, NGC 4321...) or shorter (NGC 753) than the corotation distance. Finally, when there are anomalies, such as a four-armed pattern (NGC 6814), those minima are not related at all with main resonances.

Anyway, not all features occur in any single galaxy. In some cases there are local $S_2(r)$ minima, or in the S2 image; in others there are changes in dominant mode; on other occasions pitch angle, skewness or the difference in mean position sign changes, etc. The most reliable case occurs when these features are present one at a time. One by one, they can then be produced for multiple physical processes, for example, lack of gas could provoke an $S_2(r)$ or S2 minimum, but with no a change in pitch angle dominant mode.

Fourier decomposition does not show much difference between *grand design* and flocculent galaxies. In both flocculent cases the amplitudes are very low, but they are not the lowest in the sample. Also these galaxies present a rich structure, one with *leading* arms in a *trailing* main pattern, and the other with a very important S_3 image.

Acknowledgements. We are indebted to the referee, Dr. D.M. Elmegreen, for interesting remarks. This project was partially supported by the Spanish DGICYT grant No. PB94-0433 and by the Mexican CONACyT project No. F689E9411.

References

Arsenault R., Boulesteix J., Georgelin Y., Roy J.R., 1988, A&A 200, 29

Burbidge E.M., Burbidge G.R., Prendergast K.H., 1961, ApJ 134, 874

Cepa J., Beckman J.E., 1990a, ApJ 349, 497

Cepa J., Beckman J.E., 1990b, A&AS 170, 209

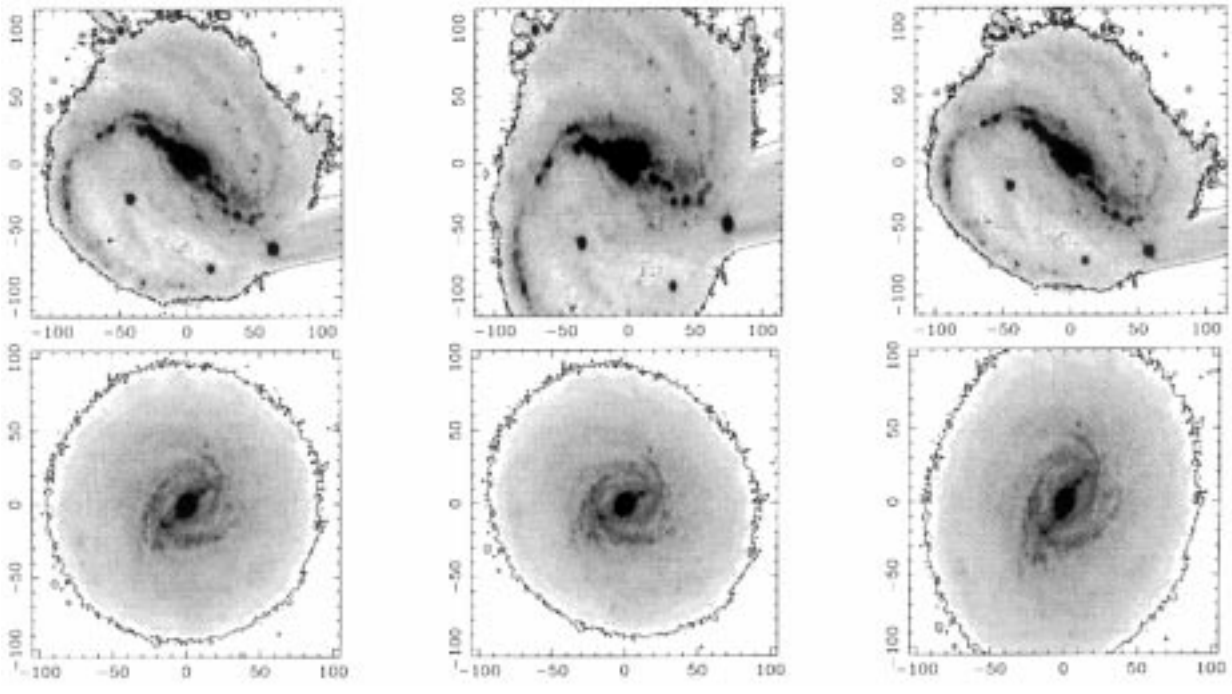

Fig. 10. (continued) NGC 7479 (top) and NGC 7723 (bottom)

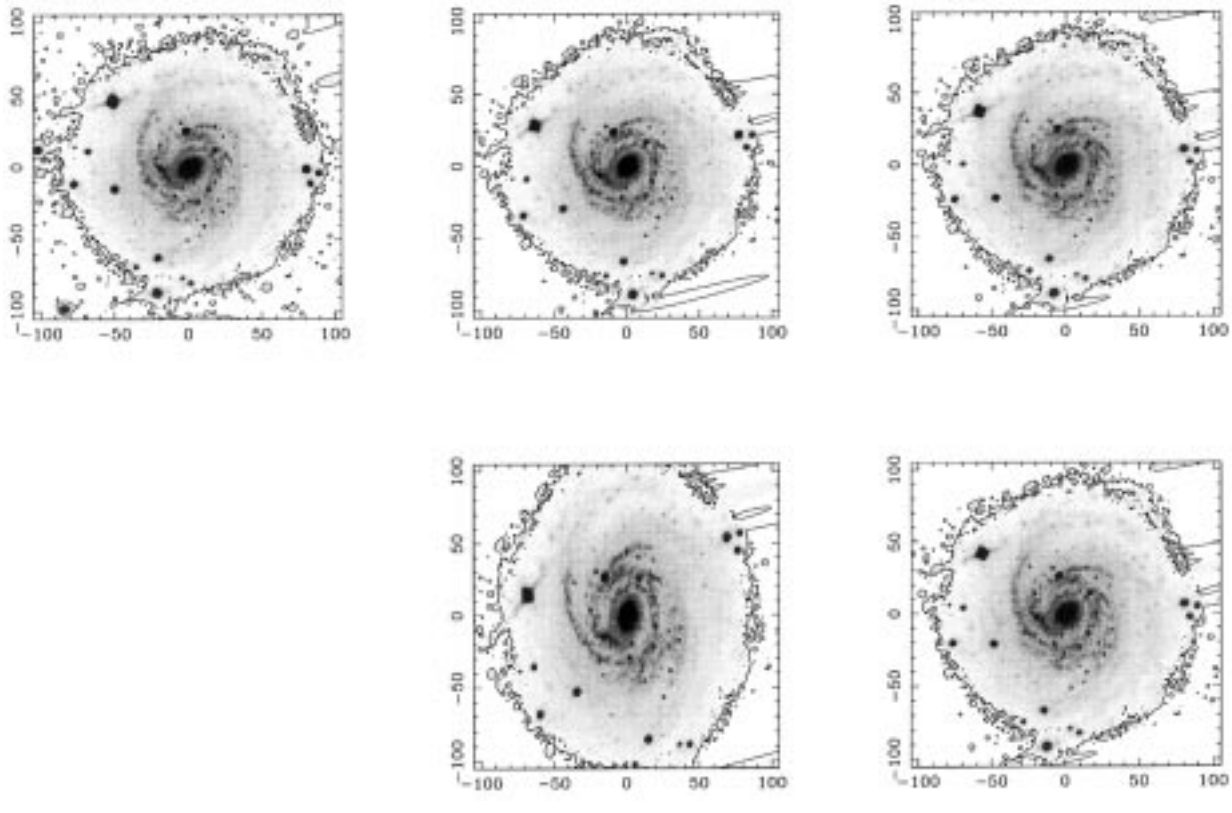

Fig. 10. (continued) NGC 6814 (deprojected following $m = 2$, upper, and $m = 4$, bottom)

Cepa J., Beckman J.E., Knapen J.H., Nakai N., Kuno N., 1992, AJ 103, 429
Cepa J., de Pablos F., 1998, ApJ (submitted)
Considère S., Athanassoula E., 1982, A&A 111, 28
Considère S., Athanassoula E., 1988, A&AS 76, 365
Danver C.G., 1942, Ann. Lund. Obs. 10, 1
de Vaucouleurs G., de Vaucouleurs A., Corwin H.G., Buta R.J., Paturel G., Fouqué P., 1991, "Third Reference Catalogue of Bright Galaxies". Springer-Verlag (RC3)
Devereux N.A., 1989, ApJ 346, 126
Eckart A., Cameron M., Jackson J.M., Genzel R., Harris A.I., Wild W., Zinnecker H., 1991, ApJ 372, 67
Elmegreen B.G., Elmegreen D.M., 1990, ApJ 355, 52
Elmegreen B.G., Elmegreen D.M., Montenegro L., 1992, ApJS 79, 37
Elmegreen B.G., Elmegreen D.M., Montenegro L., 1993, PASP 105, 644
Elmegreen B.G., Elmegreen D.M., Seiden P.E., 1989, ApJ 343, 602
Elmegreen D.M., Elmegreen B.G., 1987, ApJ 314, 3
Elmegreen D.M., Elmegreen B.G., 1995, ApJ 445, 591
Grosbøl P.J., 1985, A&AS 60, 261
Hua C.T., Donas J., Doan N.H., 1980, ApJ 90, 8
Hubble E., 1934, ApJ 79, 8
Kalnajs A.J., 1975, in "La dynamique des galaxies spirales", Weliachew L. (ed.), Colloq. Internat. CNRS 241 103
Kennicutt R.C., 1981, AJ 86, 1847
Knapen J.H., Arnth-Jensen N., Cepa J., Beckman J.E., 1993, AJ 106, 96
Lin C.C., Lau Y.Y., 1979, Stud. Appl. Math. 60, 97
Osterbrock D.E., Cohen R.D., 1982, ApJ 261, 64
Pasha I.I., 1985, Pis'ma Astron. Zh. 11, 3
Patsis P.A., Contopoulos C., Grosbøl P.J., 1991, A&A 243, 373
Patsis P.A., Hiotelis N., Contopoulos C., Grosbøl P.J., 1994, A&A 286, 46
Puerari I., Dottori H.A., 1992, A&AS 93, 469
del Río M.S., Cepa J., 1998a, A&A (submitted) (Paper II)
del Río M.S., Cepa J., 1998b, A&A 340, 1 (Paper III)
Rubin V.C., Thonnard N., Ford W.K., 1975, ApJ 199, 31
Sandage A., Tammann G.A., 1987, "A Revised Shapley-Ames Catalog of Bright Galaxies", 2nd. ed. Carnegie Institution of Washington, Washington DC
Schwarz M.P., 1984, MNRAS 209, 93
Thomasson M., Elmegreen B.G., Donner K.J., Sundelius B., 1990, ApJ 356, L13
Ulrich M.H., 1971, ApJ 165, L61
Young J.S., Devereux N.A., 1991, ApJ 373, 414
Zasov A.V., Kyazumov H.A., 1981, Pis'ma Astron. Zh. 7, 131